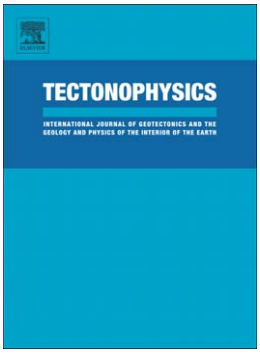

Interactions of multi-scale heterogeneity in the lithosphere: Australia

B.L.N. Kennett, K. Yoshizawa, T. Furumura

PII: S0040-1951(17)30291-3
DOI: doi: 10.1016/j.tecto.2017.07.009
Reference: TECTO 127557

To appear in: *Tectonophysics*

Received date: 5 May 2017
Revised date: 6 July 2017
Accepted date: 10 July 2017

Please cite this article as: Kennett, B.L.N., Yoshizawa, K., Furumura, T., Interactions of multi-scale heterogeneity in the lithosphere: Australia, *Tectonophysics* (2017), doi: 10.1016/j.tecto.2017.07.009

Interactions of multi-scale heterogeneity in the lithosphere: Australia

B.L.N. Kennett[a,*], K. Yoshizawa[b], T. Furumura[c]

[a]*Research School of Earth Sciences, The Australian National University, Canberra ACT 2601 , Australia*
[b]*Department of Earth and Planetary Sciences, Faculty of Science, Hokkaido University, Sapporo, Japan*
[c]*Earthquake Research Institute, The University of Tokyo, Tokyo, Japan*

Abstract

Understanding the complex heterogeneity of the continental lithosphere involves a wide variety of spatial scales and the synthesis of multiple classes of information. Seismic surface waves and multiply reflected body waves provide the main constraints on broad-scale structure, and bounds on the extent of the lithosphere-asthenosphere transition (LAT) can be found from the vertical gradients of *S* wavespeed. Information on finer-scale structures comes through body wave studies, including detailed seismic tomography and *P*-wave reflectivity extracted from stacked autocorrelograms of continuous component records. With the inclusion of deterministic large-scale structure and realistic medium-scale stochastic features fine-scale variations are subdued. The resulting multi-scale heterogeneity model for the Australian region gives a good representation of the character of observed seismograms and their geographic variations and matches the observations of *P*-wave reflectivity. *P* reflections in the 0.5-3.0 Hz band in the uppermost mantle suggest variations on vertical scales of a few hundred metres with amplitudes of the order of 1%. Interference of waves reflected or converted at sequences of such modest variations in physical properties produce relatively simple behaviour for lower

*Corresponding Author: Brian.Kennett@anu.edu.au

frequencies, which can suggest simpler structures than are actually present. Vertical changes in the character of fine-scale heterogeneity can produce apparent discontinuities. In Central Australia a 'mid-lithospheric discontinuity' can be tracked via changes in frequency content of station reflectivity, with links to the broad-scale pattern of wavespeed gradients and, in particular, the gradients of radial anisotropy. Comparisons with xenolith results from southeastern Australia indicate a strong tie between geochemical stratification and *P*-wave reflectivity.

Keywords: multi-scale heterogeneity; lithosphere-asthenosphere transition; lithospheric reflectivity; fine-scale structure; radial anisotropy.

Contents

1. Introduction

The continental lithosphere is heterogeneous on all scales from the micro-scale to the scale of a whole continent. These variations carry with them the signature of the processes that shaped the current nature of the lithosphere, yet are revealed only selectively by available geophysical and geochemical probes. The main results on heterogeneity come from the interpretation of seismological observations of different types, revealing both large-scale and finer-scale structures. Australia provides a fine laboratory for such lithospheric studies with a broad spread of crustal ages and a convenient distribution of earthquakes around and within the continent.

The broad-scale 3-D variations in the structure of the continental lithosphere, at scales longer than 300 km, are best constrained from longer-period seismic observations, exploiting the properties of surface waves and multiply reflected *S* body waves, with global coverage (e.g., Schaeffer and Lebedev, 2013). At the regional scale with a good distribution of sources and seismic stations, it is possible to achieve horizontal resolution of the order of 200 km (e.g., Yoshizawa, 2014). This is also the scale at which the pattern of heterogeneity in multiple regional models using dense data are consistent (Becker, 2012), though variations in the amplitude of wavespeed variation are apparent between models. Cratonic zones are commonly underlain by fast wavespeed anomalies, with a typical lithospheric thickness of about 200 km. In Australia, tomography exploiting the large amplitude parts of seismograms from regional sources provide evidence for strong radial anisotropy with faster *SH* wavespeed than *SV* in the asthenosphere, but also at shallower depths above 90 km (Yoshizawa, 2014). The strength of radial anisotropy tends to be weak in the middle to lower lithosphere.

Body wave tomography exploiting relatively dense deployments of portable seismic recorders provides information on the lithospheric mantle at shorter scales. Potential horizontal resolution is limited by station spacing (Rawlinson et al., 2014), but vertical smearing due to the relatively narrow cone of incoming rays also limits resolution in the upper mantle. The comprehensive deployment of the

USArray across the continental United States, with a station spacing of around 70 km, has provided detailed information on both crustal and upper mantle structure (Shen and Ritzwoller, 2016). The suite of portable instrument deployments in the WOMBAT project in southeastern Australia, demonstrates the presence of considerable complexity beneath the crust (e.g., Rawlinson et al., 2014) with variations down to the available sampling of 50 km.

The presence of much finer-scale structure in the mantle is indicated by long trains of high-frequency *P* and *S* waves following the phases *Pn* and *Sn* refracted back from the mantle. An example is shown in Figure 1 for a continental path within Australia.

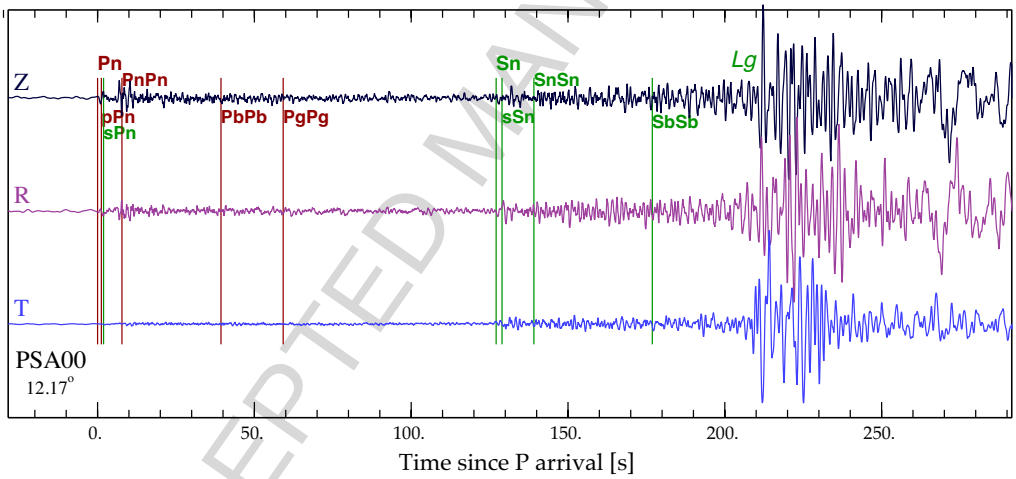

Figure 1: Three component seismogram at the central element of the PSAR array in northwestern Australia from the 2012 Mw 5.2 Ernabella event in Central Australia at 12.17° epicentral distance. Extended high frequency coda for both *P* and *S* waves is present on all three components indicative of a strong scattering environment. The phases are marked for a regional model – 9 s faster for *S* than the *ak135* reference model (Kennett et al., 1995).

1.1. Crustal heterogeneity

In many parts of the world the continental crust is well characterized using both active and passive seismic techniques. Major divisions of crustal structure are recognisable, frequently with a strong link to the age of formation or accretion. Within the major crustal units, reflection seismology reveals fine scale structure

superimposed on the major changes in seismic wavespeed. This fine structure arises from variations in *P* wavespeed or density that lead to localized impedance contrasts.

Australia is well sampled by full-crustal reflection surveys in a wide range of geological environments (Kennett et al., 2016). In the crystalline crust most reflector segments appear quite short, no more than a kilometre or so, but in aggregate can build to bands of significant reflectivity. The reflectivity patterns are distinctive (e.g., Kennett and Saygin, 2015), and are likely to be linked to the processes of crustal assembly, since differences appear in blocks with different geological provenance. At the frequencies used in reflection work ($>$ 10 Hz) the upper mantle is generally transparent though there are a few places with very distinct inclined reflections at depth, often interpreted as fossil subduction zones (Warner et al., 1996; Hammer et al., 2010).

1.2. Lithospheric mantle

Complex structure with localised velocity increase at the base of the lithosphere has been inferred from the properties of refracted seismic waves (e.g., Kennett and Bowman, 1990) from earthquake sources, with a low wavespeed and higher attenuation zone beneath – characteristic of the asthenosphere. Similar complex wavespeed profiles have also been inferred from the interpretation of long profiles across the former Soviet Union using peaceful-nuclear explosions (PNE) (e.g., Mechie et al., 1993). On these profiles, high frequency *Pn* arrivals can be tracked out to more than 2500 km from the source (e.g., Morozov et al., 1998).

The *P* wave arrivals from a range of large-scale controlled source experiments have been analysed to suggest a significant boundary in the lithosphere in cratonic regions at about 90 km depth. This boundary was termed the 8° discontinuity by Thybo and Perchuc (1997), and may also correspond to the mid-lithosphere discontinuity inferred from receiver function studies (e.g. Ford et al., 2010). The lower part of the lithosphere beneath the discontinuity has also been suggested to be a slight seismic low velocity zone compared with its surroundings (e.g. Thybo,

2008). These studies have mostly worked with 1-D velocity profiles, so that the possibility exists that 3-D structure has been mapped into apparent complexity in the wavespeed profile with depth.

Even before the advent of extensive seismic tomography, the presence of heterogeneous features in the mantle with scale lengths of the order of 100 km was inferred from patterns of amplitudes of seismic events (Kennett and Bowman, 1990). Kennett and Nolet (1990) showed that such medium-scale structure is largely transparent to the waves employed in surface wave tomography, and so the broad-scale results are not affected. With the use of full-waveform inversion techniques working directly in 3-D, the potential exists for incorporating structures on many scales from their influence on seismic waveforms over a broad ranges of frequencies, but so far this is only achievable where very dense station deployments are available within an already well characterized region (Fichtner et al., 2013a).

1.3. Fine-scale structure in the lithospheric mantle

The current information on fine-scale structure in the lithosphere is somewhat limited, and has been strongly influenced by the nature of the high-frequency *P*-arrivals travelling 2000 km or more on the well-sampled long profiles across the former Soviet Union obtained using peaceful-nuclear explosions (PNE).

A number of different styles of model have emerged from analysis of these arrivals and their long coda, with focus on different classes of *P*-arrivals and distance ranges. Somewhat divergent views have emerged from these studies on the seismic character of the sub-continental mantle lithosphere.

Thus Tittgemeyer et al. (1996) introduced a stochastic model with strong quasi-laminar structure in the top 100 km of the lithospheric mantle as a means of ducting high-frequency energy to long distances. In contrast Nielsen et al. (2003) emphasized the role of crustal scattering, dominantly from the base of the crust, linked to multiply reflected *P* waves in the mantle returned from a significant velocity gradient in *P* wavespeed ('whispering gallery' phases). Modelling by Nielsen and Thybo (2003) demonstrated that this class of model

with a horizontally uniform mantle structure could provide a good representation of the onsets of the *P* waves on the QUARTZ profile across Eurasian Russia. Their preferred model does not include any significant fine-scale heterogeneity down to 130 km, but has a more heterogeneous zone below where *P* wavespeeds decrease (Thybo, 2008).

Rather than employ a stochastic model Morozova et al. (1999) have exploited the full range of *P* wave observations for the profile QUARTZ across Eurasian Russia, including intermediate smaller shots, and have built up a complex deterministic structure through the full lithosphere. Their results indicate the important role played by horizontal gradients in *P* wavespeed and the presence of some localized low velocity zones within the generally faster lithosphere. The presence of such broad-scale variations in seismic wavespeed have an impact on the patterns of multiple *P* reflections beneath the Moho. The bounce points of different levels of underside multiple reflections in 'whispering gallery' phases will not coincide in the presence of the lateral heterogeneity giving rise to a more complex pattern of behaviour with less consistent phase groups.

A different class of information on lithospheric structure is provided by high-frequency observations of *P* and *S* phases, with very long coda, from events in the Indonesian subduction zones recorded in northern Australia (Kennett and Furumura, 2008) and for Australian events recorded at seismic stations on the cratons. In Figure 1 we illustrate the nature of the seismograms for the Mw 5.2 event near Ernabella in central Australia as seen on a path to the northwest. There are distinct differences in the character of the seismograms for cratonic paths with higher frequencies and earlier arrivals than for paths traversing the Phanerozoic domains to the east. The nature of the extended high-frequency coda, particularly for paths within the Precambrian domains, requires some form of distributed heterogeneity through the lithosphere, though not necessarily uniform (cf. Kennett and Furumura, 2008).

1.4. Lithospheric discontinuities

Receiver function studies have been widely applied to extract the wave conversions and reflections underneath seismic stations. Discontinuities in seismic properties of the lithosphere are then inferred from the character of the receiver function time series. The Moho is normally well constrained, except where the transition from crust to mantle is gradational. However, for incident *P* waves the conversion from interfaces inside the mantle lithosphere can be obscured by crustal multiples (Rychert and Shearer, 2009). Such interference does not occur for incident *S* waves for which the converted *P* waves arrive as precursors to the main *S* phase, but here lower frequency waves have to be used so that resolution is limited.

One of the striking features in *S*-wave receiver function analysis for the Australian cratons is clear signals of discontinuities in the mid-lithosphere at around 70-90 km (Ford et al., 2010), which may indicate a rapid drop in seismic velocity or a change in the character of radial anisotropy in the middle part of the continental lithosphere where the wavespeed is generally at its fastest. The estimated depth of the enigmatic mid-lithosphere discontinuity (MLD) from receiver functions corresponds well with a rapid change in the strength of radial anisotropy derived from surface waves (Yoshizawa and Kennett, 2015).

An additional constraint on the nature of lithospheric heterogeneity comes from observations of high-frequency *P*-wave reflectivity profiles derived from the autocorrelograms of vertical component records at seismic stations across Australia (Kennett, 2015). These *P* reflectivity profiles suggest vertical changes in the character of the fine-scale structures in the Australian continent, indicating stronger reflectivity in the crust and upper lithosphere underneath the cratons. Such observations support the existence of fine-scale laminated heterogeneity in the lithosphere superimposed on broader-scale wavespeed variations. Such behaviour was suggested from numerical simulations of high-frequency scattering of seismic waves for the paths in the cratonic areas (Kennett and Furumura, 2008). Recently Kennett and Furumura (2016) have undertaken a further suite

of numerical studies covering the full range of tectonic environments across the Australian continent and have been able to demonstrate good correspondence between the numerical simulations and the properties of both high-frequency refracted waves and *P* wave reflectivity.

The presence of such quasi-laminar fine-scale heterogeneity in the lithosphere has equivalent effects to shape-preferred orientation of crystals, and so vertical variations in the character of the heterogeneity can produce changes in the effective radial anisotropy for long-wavelength surface waves as well as apparent discontinuities in the mid-lithosphere region for higher frequency body waves.

The base of the seismic lithosphere is often difficult to recognise because there is no sharp contrast to the asthenosphere beneath. A variety of approaches have been used to provide a single depth estimate for the lithosphere-asthenosphere boundary (LAB), even though a gradual transition is more likely. Methods include the depth to the maximum velocity gradient (e.g. van der Lee, 2002), the depth to a certain velocity anomaly above a global reference model (e.g. Simons et al., 2002), and estimates based on conversion from wavespeed to temperature with an isotherm as a proxy for the LAB (e.g. Fishwick, 2010).

The gradational nature of the transition from lithosphere to asthenosphere would account for the absence of any clear signal from the base of the lithosphere beneath central and western Australia in the Sp receiver function study of Ford et al. (2010), even though MLD arrivals are seen. In the east the transition is sharper, and the LAB is imaged in the receiver function work.

In this study we employ bounds on the lithosphere-asthenosphere transition (LAT) across Australia extracted from the character of vertical velocity gradients from the surface wave inversion of Yoshizawa (2014). Changes in the depth span between these bounds link to the major tectonic elements of the continent.

1.5. Multi-scale interaction

In this contribution we bring together a range of information on the character of lithospheric wavespeed variability across Australia from surface waves and body waves spanning a broad range of frequencies. The integration of the full

range of heterogeneity results, with the aid of numerical simulation, leads to the development of multi-scale heterogeneity models for the lithosphere. Such models with a wide range of length scales allow us to investigate the way in which the finer-scale structure of the lithosphere can manifest in results at moderate to low frequencies. We show that the interaction of the different scales of heterogeneity can have significant effects on the character of seismic wave propagation, which are then manifest in the interpretation of seismological observations.

Individual seismic probes illuminate different aspects of the heterogeneity, but the full spectrum has to be taken into account to understand the properties of apparent discontinuities and their geodynamic implications. Once fine-scale structure is taken into consideration it becomes apparent that wave interference plays a very important role in determining the nature of apparent discontinuities seen with lower frequency probes such as *S* wave receiver functions. Changes in the character of fine-scale heterogeneity as a function of depth can themselves produce apparent discontinuities.

Although geochemical probing of the lithosphere is limited by access to direct samples, analysis of xenoliths can provide valuable information about chemical and mineralogical zonation. We are able to compare results from a suite of xenoliths across southeastern Australia tracking form the South Australian craton into the Phanerozoic domains with estimates of *P* wave reflectivity. We find a close correspondence between the depths of chemical change and variations in reflectivity suggesting a direct link between mineralogical variation and zonation with the seismic properties of the lithosphere.

2. The Australian lithosphere

The exposed geology of the Australian continent is composed of an assemblage of crustal blocks that can be broadly grouped into the Precambrian western and central cratonic zones and the Phanerozoic eastern province (Figure 2). The Australian continental crust was accreted in three major episodes, that

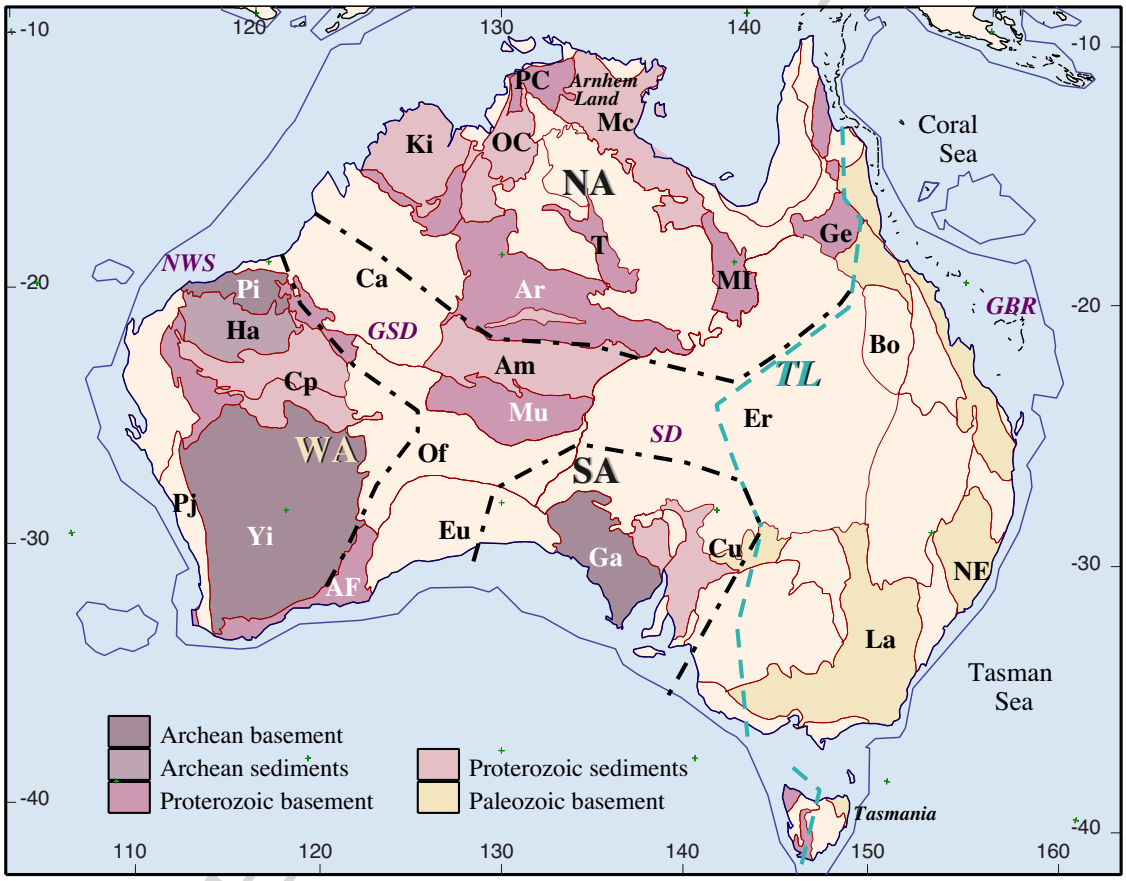

Figure 2: Simplified relationships of major tectonic features of Australia. The outlines of the major cratons are indicated: WA – West Australian Craton, NA – North Australian craton, SA – South Australian craton, and TL – the Tasman Line marking the limit of Precambrian exposure. Marked features: AF AlbanyFraser Orogen, Ar - Arunta Block, Am - Amadeus Basin, Ca - Canning Basin, Co Cooper Basin, Cp - Capricorn Orogen, Cu Curnamona Craton, Er - Eromanga Basin, Eu - Eucla Basin, Ga - Gawler Craton, Ge -Georgetown Inlier, Ha - Hamersley Basin, Ki - Kimberley block, La Lachlan Orogen, Mc - MacArthur Basin, MI - Mt Isa Inlier, Mu - Musgrave Orogen, NE - New England Orogen, Of - Officer Basin, PC - Pine Creek Inlier, Pi - Pilbara Craton, Pj - Pinjarra Orogen, T - Tennant Creek Inlier, Yi - Yilgarn Craton; SD - Simpson Desert, GSD - Great Sandy Desert, GBR Great Barrier Reef, NWS North West Shelf.

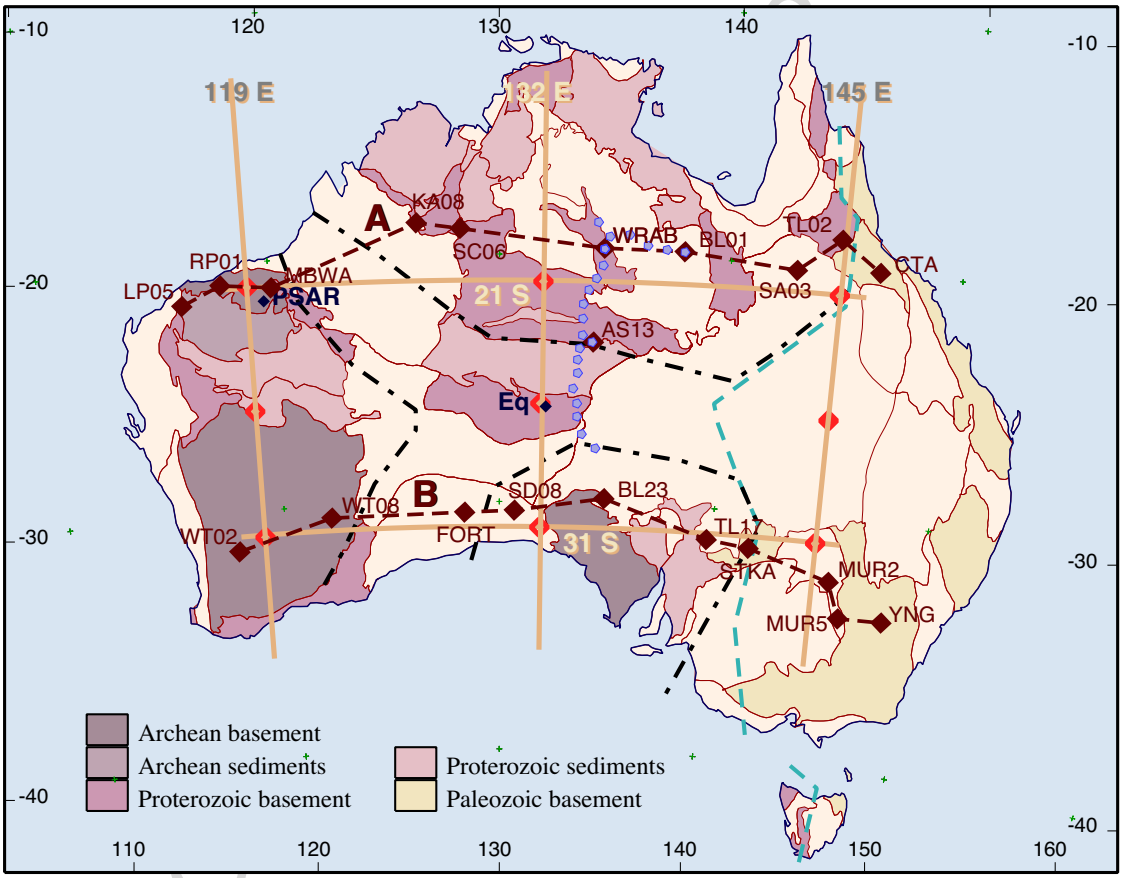

Figure 3: The location of the lines A, B of P-wave reflectivity across multiple stations illustrated in Figure 6, and the configuration of the profiles used for numerical simulation of multi-scale heterogeneity (light brown). The locations of the heterogeneous segments discussed in Section 3 are denoted by red markers. The positions of the 2012 Ernabella earthquake and the PSAR array in northwestern Australia are also indicated, the seismogram is shown in Figure 1. The light blue symbols indicate the locations of the suite of stations used in the study of the mid-lithospheric discontinuity in Central Australia in Section 5.

each assembled one third of the continental area. This started with the Archean cratons in the west, with the Phanerozoic provinces in the east added in the last stage.

Disparate Archean crustal elements were assembled into three major cratonic zones in the Proterozoic; West Australia, the North Australian Craton and the South Australian Craton were formed by 1830 Ma, and these cratonic elements were joined to the Rodinian supercontinent by 1300–1100 Ma (Cawood and Korsch, 2008). This supercontinent broke up around 800 Ma. Subsequently, the fold belt structures of the Phanerozoic Tasman Orogen of the eastern third of Australia were accreted onto the eastern margin of the Precambrian cratons during the Palaeozoic in a series of stages (e.g., Direen and Crawford, 2003).

The east of Australia was an accretionary margin through the Palaeozoic with a sequence of subduction complexes on the East Gondwana margin, progressively building to the east. Australia parted company with East Antarctica by around 80 Ma, and later the opening of the Tasman Sea from 80 to 60 Ma separated the Lord Howe Rise from eastern Australia to leave a submerged continental ribbon (see, e.g., Gaina et al., 1998). Since 40 Ma there has been significant volcanism in eastern Australia, with a mixture of lava fields and age-progressive volcano chains. Neogene volcanism along the eastern margin has left chains of volcanic edifices on land and in the Tasman sea (Davies et al., 2015), with eruptions as recent as 4000 BCE at Mt Gambier (38°S, 141°E).

In Figure 2 we show a simplified model of the tectonics of Australia, with an indication of the age of the major elements. The areas in the lightest tone have extensive regolith cover with very little outcrop, but even in the areas indicated by darker tones outcrop can be patchy. The cratonic boundaries are based on the work of Cawood and Korsch (2008), and the Tasman Line on the reinterpretation by Direen and Crawford (2003). The original concept of the Tasman Line was based on the easternmost outcrop of Precambrian material, but such outcrop is limited along much of the length. Many different interpretations have been invoked based on lineations derived from potential field measurements (gravity, magnetics) that

are likely to arise from features in the upper part of the crust. The Tasman Line has been related to the edge of the continent at the time of break-up of Rodinia, but in the mantle the main contrasts lie somewhat to the east as noted by Kennett et al. (2004).

In addition to the tectonic information we display in Figure 3 the northern (A) and southern (B) lines of seismic stations for which we present lithospheric *P*-wave reflectivity in Figure 6. We also indicate the configuration of the grid of profiles employed in the numerical simulation that allowed the development of of multi-scale heterogeneity models (Kennett and Furumura, 2016), discussed in Section 3. The locations at which detailed heterogeneity segments have been extracted are indicated with red markers.

2.1. Large-scale structure

The configuration of earthquake belts around Australia provide a good distribution of events at regional distance, particularly from the subduction zones to the north and east. There are much less events from the mid-ocean ridge between the Australian and Antarctic plates to the south, and only a few to the west of Australia. This wealth of regional seismograms has been exploited in a number of studies of the upper mantle beneath Australia that exploit the large amplitude surface waves and multiple S waves in the later parts of seismograms. These studies have exploited recordings at portable broad-band seismic stations and the limited number of high-quality permanent stations (see, e.g., Debayle and Kennett, 2003). The period range employed is generally from from 20 to 200 s.

A variety of techniques have been employed to extract information on 3-D structure from the seismic waveforms. One approach is to extract path-specific velocity models using either direct inversion (e.g., Simons et al., 2002), or secondary variables that improve the linearity of the inversion (e.g., Debayle and Kennett, 2003; Fishwick et al., 2005). These path-based models are then combined with a linear inversion to produce 3-D shear wave speed structure. An alternative approach via the construction of phase speed maps for multiple modes and frequencies allows the incorporation of finite-frequency sampling

(Yoshizawa and Kennett, 2004). A fully non-linear inversion of the waveforms using 3-D models from the outset has been employed by Fichtner et al. (2009, 2010). This computationally intensive approach uses the spectral element technique for modelling the wave propagation and adjoint methods to extract the necessary derivatives, which include all finite-frequency effects. Although there are noticeable difference between different models, the longer spatial wavelength components are very consistent (Fichtner et al., 2012). The Australian Seismological Reference Model (AUSREM) provides a representative model for the lithospheric mantle building on a number of the earlier studies (Kennett et al., 2013).

Yoshizawa (2014) has recently developed a new radially anisotropic 3-D shear wave model for Australia from a large number of multi-mode surface wave paths across Australia, based on multi-mode phase speed measurements (Yoshizawa and Kennett, 2002a; Yoshizawa and Ekström, 2010), with the incorporation of finite-frequency effects (Yoshizawa and Kennett, 2002b, 2004). The plausible depth range of the lithosphere-asthenosphere transition (LAT) is estimated by exploiting the character of the wavespeed gradients on local vertical profiles through the 3-D shear wavespeed model. The shallower bound is taken where the negative vertical gradient in isotropic wavespeed is largest. The deeper bound is placed at the minimum absolute wavespeed beneath the lithosphere, and thus the minimum of the *S* wave low velocity zone (Yoshizawa, 2014). With this definition, the LAT lies in a low-velocity-zone created by the high shear wavespeeds in the shallower part of the lithosphere. The shallower bound generally lies just below the highest *S* wavespeeds.

For a number of parts of the continent even the deeper bound on the LAT lies somewhat shallow than the lithospheric thickness in the global *Litho1.0* model of Pasyanos et al. (2014). The inclusion of higher modes of the surface waves in the Australian regional study (Yoshizawa, 2014) improves resolution of gradients in both depth and horizontally.

The vertical wavespeed profiles are extracted on a 0.5° grid and the shallower

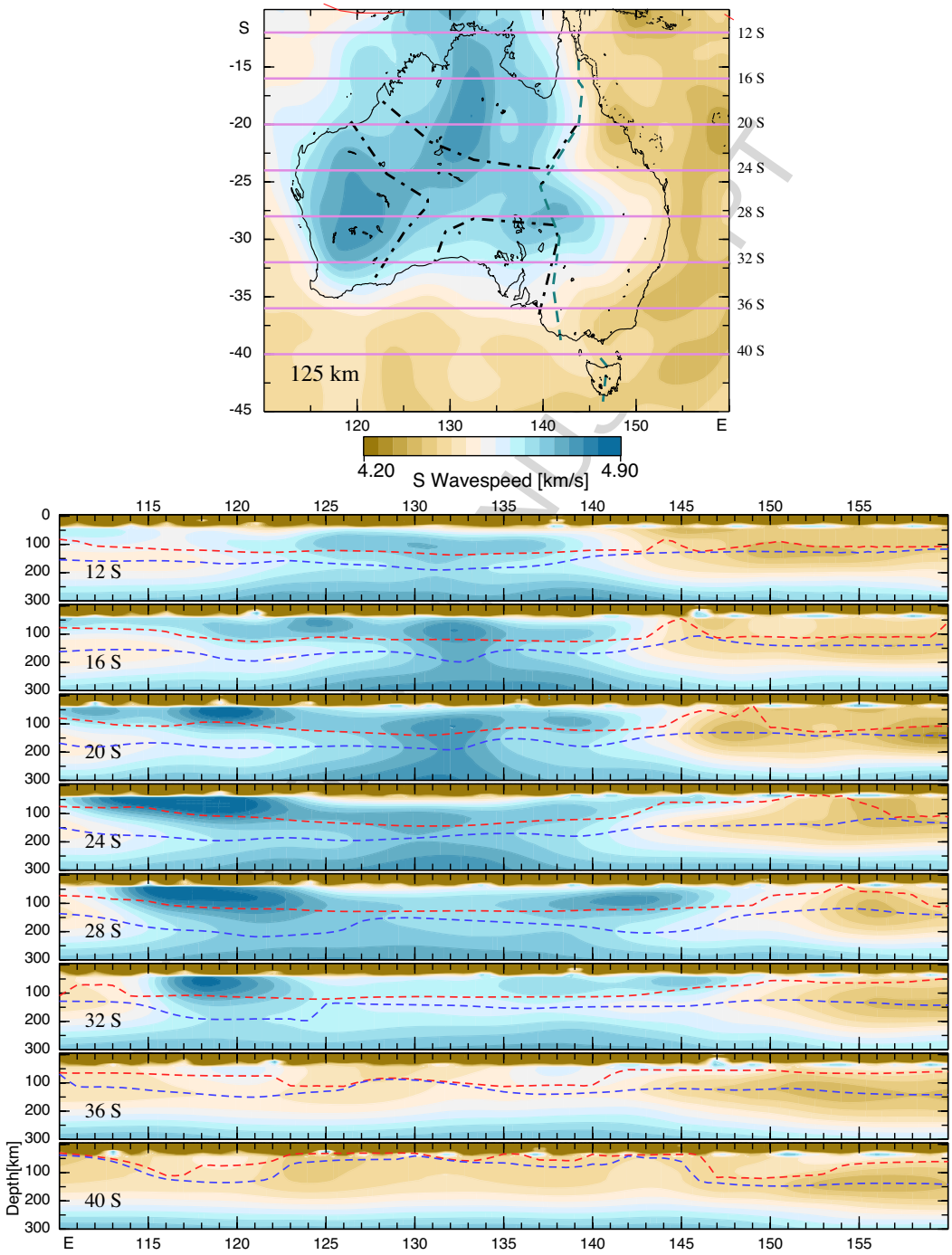

Figure 4: The distribution of isotropic *S* wavespeed for the model of Yoshizawa (2014) at 125 km depth in the upper panel, together with cross-sections at constant latitude with the shallow and depper bounds on the lithosphere-asthenosphere transition (LAT) indicated by red and blue dashed lines. The outlines of the cratons and the location of the Tasman Line are indicated in the upper panel.

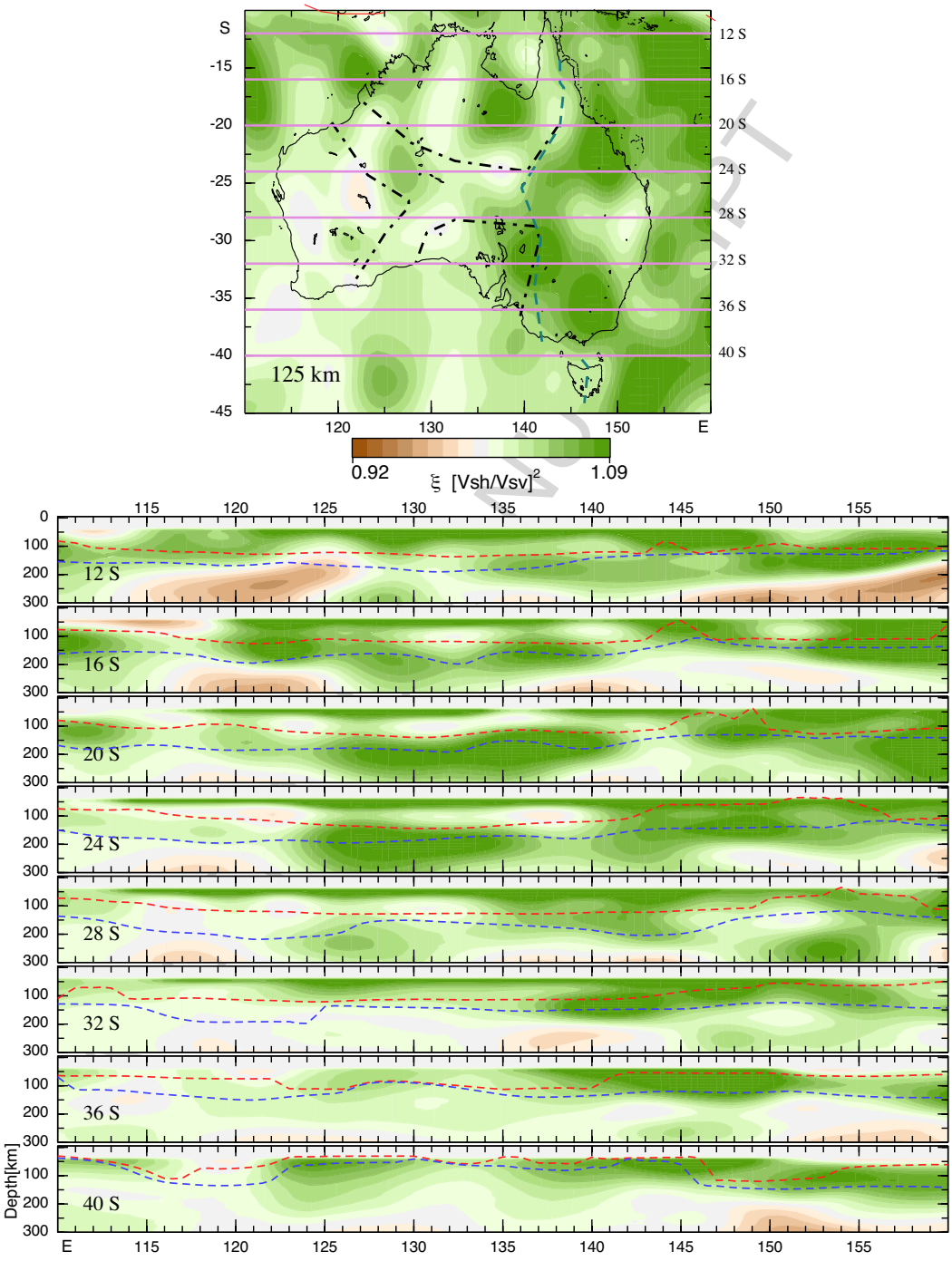

Figure 5: The distribution of radial anisotropy for the model of Yoshizawa (2014) at 125 km depth in the upper panel, together with cross-sections at constant latitude with the shallow and depper bounds on the lithosphere-asthenosphere transition (LAT) indicated by red and blue dashed lines. The outlines of the cratons and the location of the Tasman Line are indicated in the upper panel.

and deeper LAT bounds are estimated at each of these grid positions. The bounds on the LAT are particularly effective in zones of thick lithosphere, though they will tend to exaggerate the thickness of the transition when it is very sharp (Yoshizawa, 2014). For thick cratonic lithosphere the deeper bound correlates well with other ways of estimating the depth to the base of the lithosphere. Whereas, for thinner lithosphere the shallower bound tends to lie closer to alternative estimates of lithospheric thickness; in such areas the deeper bound marks the lowest wavespeed encountered in the asthenospheric low velocity zone beneath.

With this representation of the transition between the lithosphere and the asthenosphere we can examine lateral variations and the relation with alternative lithospheric properties. We consider both the wavespeed and radial anisotropy of the Yoshizawa (2014) model, together with discontinuities extracted from the analysis of receiver functions across Australia (Ford et al., 2010).

We display the isotropic S wave speed and radial anisotropy of the continental lithosphere of Australia in Figures 4 and 5. In addition to maps of the properties at 125 km depth with superimposed outlines of the cratons and the Tasman Line, we show west-to-east sections at constant latitude at 4° intervals. These vertical cross sections cover the full range of tectonic provinces in Australia. As can be readily seen in 4 and 5 the major contrasts in the mantle lithosphere lie somewhat to the east of the inferred position of the Tasman Line, as earlier noted by Kennett et al. (2004).

The shallower bound on the LAT indicated with red dashed lines in Figures 4 and 5 appears flat across the Archean and Proterozoic regions of the continent, confined to the depth range between 120 and 150 km. In the east of Australia the bounds on the LAT tend to diverge with the shallow bound marking the top of the strong gradient associated with a relatively sharp transition as seen in the *Sp* receiver function results (Ford et al., 2010).

In contrast, the deeper bound on the LAT indicated by blue dashed lines in Figures 4 and 5 clearly displays large regional variations from 160 to 250 km. The deepest locations for this bound are associated with the rather thick lithosphere

beneath the Yilgarn Archean craton in western Australia, as well as in the center of northern Australia. The thickness of the LAT is large in the West Australian craton, while in South Australian craton and the Mesoproterozoic suture zones the LAT appears somewhat thinner. In the cross-sections at 24-32°S we clearly see the thick cratonic lithosphere beneath the West Australian craton, accompanied by a thick transition zone from lithosphere to asthenosphere. Similar features are visible for the North Australian craton on the sections for 16-20°S. The LAT is somewhat thinner in the Mesoproterozoic suture zone in central Australia and the South Australian Craton (24-32°S).

In a few places we note rather rapid changes in the estimate of the thickness of the LAT zone, such as at the edge of the Western Australian craton at 28°S and 32°S. Although such rapid transitions lie at the limit of potential resolution, they tie well in location to other geophysical information, e.g. gravity, indicating a distinct change in the character of the lithosphere.

It should be noted that in the oceanic regions to the south and east of Australia the requisite velocity gradients are difficult to estimate. As a result, the apparent sharpness of the lithosphere to asthenosphere transition might be exaggerated on the sections at 36°S and 40°S between 125°E and 135°E.

For radial anisotropy (Figure 5) we see that at 125 km there is strong anisotropy with faster *SH* wave speed in eastern Australia, mostly to the east of the Tasman Line. There is a distinct patch with faster *SH* wavespeed around the triple junction among the three cratonic blocks, which merged together at about 1.3 Ga (Myers et al., 1996), but only a modest effect in isotropic *S* wavespeed. The cross sections of radial anisotropy also display faster *SH* wavespeed anomalies in the asthenosphere beneath the LAT (e.g., at 20-24°S) which may reflect horizontal shear flow beneath the fast moving Australian lithosphere as suggested by global studies (e.g. Gung et al., 2003; Debayle et al., 2005). Moderate anisotropy in the lithosphere is largely confined to the Mesoproterozoic suture zone between the major cratons, while anisotropy in the Archean and Proterozoic cratons, particularly around 100 km depth, is relatively weak. Flow beneath the lithosphere

may influence the thickness of the LAT beneath central and northern Australia.

In the cratonic blocks, particularly beneath the Pilbara and Yilgarn cratons in western Australia and the centre of the North Australian craton, the apparent LAT thickness exceeds 80 km (Figures 4 and 5). However, the Gawler craton in South Australia shows distinctly thinner lithosphere and a LAT with rather subtle differences from the suture zone in central Australia. Furthermore, the isotropic shear wave speed at the bounds of LAT beneath this region is apparently slower than for the other cratons. These differences may be associated with basal erosion during the continental breakup of Australia and Antarctica.

Yoshizawa and Kennett (2015) noted that the vertical profiles of radial anisotropy show a strong correlation with the mid-lithosphere discontinuity results obtained by Ford et al. (2010) using *Sp* receiver functions. In the West and North Australian cratons, the radial anisotropy parameter $\xi = V_{sh}^2/V_{sv}^2$ is high ($\sim$1.08) just below the base of the crust but drops with depth, usually reaching a minimum or an inflection point very close to the discontinuity depths inferred from *S* wave receiver function analysis. For the northern group of stations considered by Ford et al. (2010), ξ rises again from the minimum and remains above unity to below the deeper bound on the LAT. Yet, for the southern group of stations, there is little change below the inflection point in ξ, and radial anisotropy remains weak through the full thickness of the LAT.

2.2. Finer-scale structure

Kennett (1985) drew attention to the characteristics of high-frequency body waves from events in the Indonesian subduction zone recorded at the Warramunga array in the middle of the North Austraian craton. From shallow sources, the seismograms show very little difference in frequency content between *P* and *S* and extended complex coda, so that *S* arrives before the *P* coda has subsided. Similar effects are also seen for continental paths within cratonic Austalia, as illustrated in Figure 1. These features suggest that the arriving waves have travelled through a complex scattering environment with very low intrinsic attenuation. Gudmundsson et al. (1994) demonstrated the major difference between such

high-frequency waves trapped in the lithosphere and body wave phases returned from the upper mantle transition zone, which showed much lower frequencies indicating passage through significant attenuation beneath the lithosphere.

Such complex high-frequency arrivals are a feature of propagation to stations in the West and North Australian cratons from the front of the Indonesian subduction zone. Kennett and Furumura (2008) undertook a detailed study and were able to demonstrate that quasi-laminar heterogeneity in the lithosphere is able to produce records that match the character of the observations. They employed a stochastic model with a von Karmán distribution, using a horizontal correlation length of 20 km and vertical correlation length of 0.5 km in the lithospheric mantle. The r.m.s. amplitude levels were 2% in the upper part of the cratonic lithosphere and 1% below 100 km. The propagation paths studied included both oceanic and continental components, and Kennett and Furumura (2008) were able to show that the decay characteristics of the coda correlated well with the changes in structure in the neighbourhood of the subduction zone.

Kennett and Furumura (2016) have developed multi-scale models of heterogeneity concentrating on propagation within the Australian continent. Their work indicates the way in which heterogeneity at various levels within the lithosphere interact to produce the observed effects. The broad-scale variations, revealed by surface wave tomography, produce significant variations in the vertical gradients in the mantle beneath the crust along a long profile. As a result the subtle interference needed to produce 'whispering gallery' phases is distorted, and so it is unlikely that any part of the lithosphere is free of heterogeneity.

Observations of seismic phases refracted back from the lithosphere include the integrated effect of the entire path, including any multiples, and so it is hard to disentangle the influence of different aspects of the structure. Fortunately, it has recently become possible to obtain a more direct view of fine-scale structure in the lithosphere from estimates of high-frequency *P*-wave reflectivity beneath seismic stations extracted from stacked autocorrelograms of vertical component records (Kennett, 2015).

These estimates of *P*-wave reflectivity are constructed using the approach initiated by Gorbatov et al. (2013) using the full time series at each station. They thus include an ambient noise component equivalent to having a source and a station at the same location, and a contribution from distant earthquakes arriving at the receiver from beneath. The autocorrelation of transmitted waves to the free surface provides the reflection response below the receiver. The tests made by Kennett (2015) indicate that the dominant contribution comes from structure beneath the station, and that the results are stable in time. Nevertheless, the ambient noise contribution can include scattered energy from the sides that arrives with a delay equivalent to an origin in depth.

The *P*-wave reflectivity results include full free surface effects. For these steeply travelling *P* waves the reflection coefficients are small, so surface multiple wavetrains rapidly diminish in amplitude. This is contrast to the situation for *P* receiver functions where the converted *S* waves can have complex interactions with low wavespeed structures near the surface producing strong multiple trains. In consequence, good *P*-reflectivity results can be obtained for stations such as FORT, in southern Australia, where the *P*-receiver function does not even reveal the Moho (Ford et al., 2010).

In Figures 6, 7 we illustrate results for two profiles across northern and southern Australia (lines A and B in Figure 1), displaying the *P* reflectivity as a function of time, with an approximate conversion to depth using the *ak135* model (Kennett et al., 1995). The crustal age for each station is indicated with a coloured background, keyed to the tectonic provinces in Figure **??**. For each profile we show a cross-section through the Yoshizawa (2014) *S* wavespeed model along a parallel of latitude passing through the group of stations, the position of each station is projected to the cross-section.

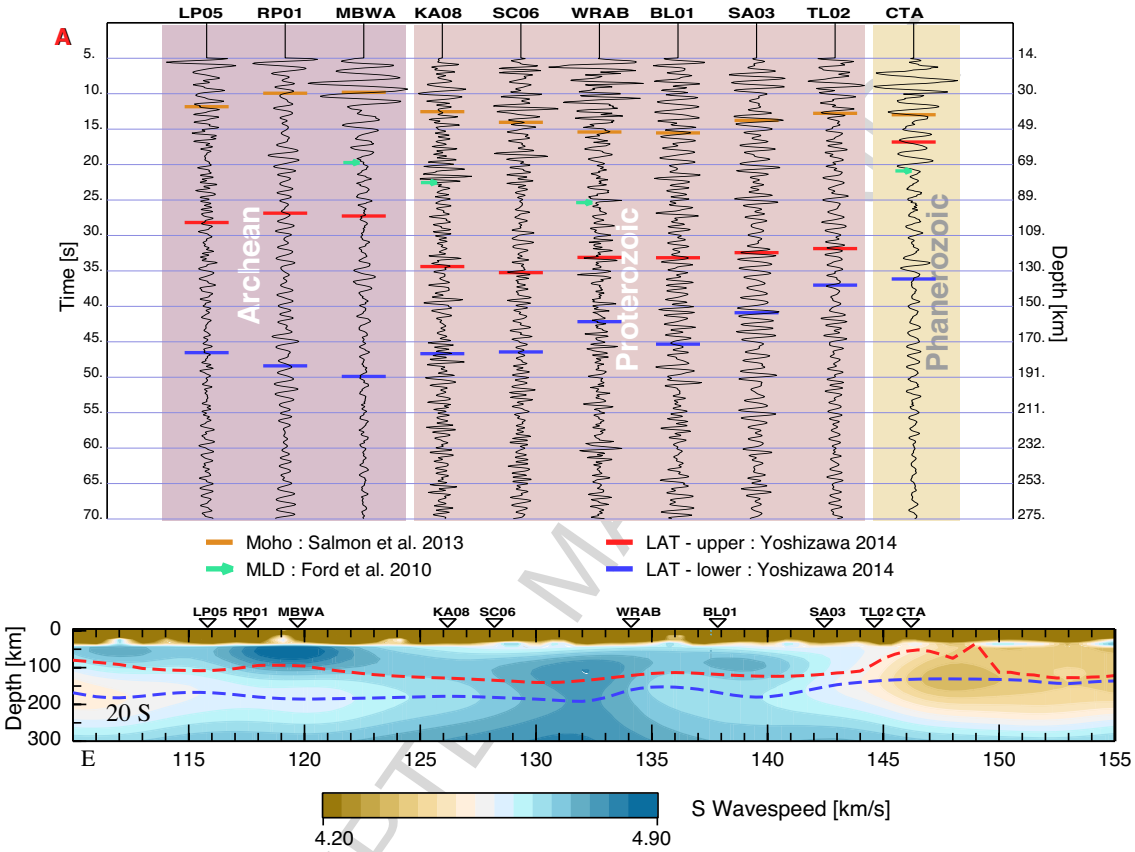

Figure 6: Estimates of *P*-wave reflectivity for stations along the northern profile **A**, for the frequency range 0.6-3.0 Hz extracted from stacked station autocorrelograms. A representative section through the isotropic *S* wavespeed model of Yoshizawa (2014) is shown below, on which the upper and lower bounds on the lithosphere-asthenosphere transition (LAT) are indicated, along with the projection of the station locations. The P wave reflectivity to 70 s two-way-time is shown, with the expected time for the Moho from the compilation of Salmon et al. (2013) and the mapping of the upper and lower bounds on the LAT are marked. Where available, arrow markers indicate the discontinuities determined by Ford et al. (2010) using *S*- wave receiver functions. The time to depth conversions are made with the *ak135* model of Kennett et al. (1995), and the depth scale is indicated at the right side of each profile. The coloured backgrounds indicate the broad age provinces from Figure 2.

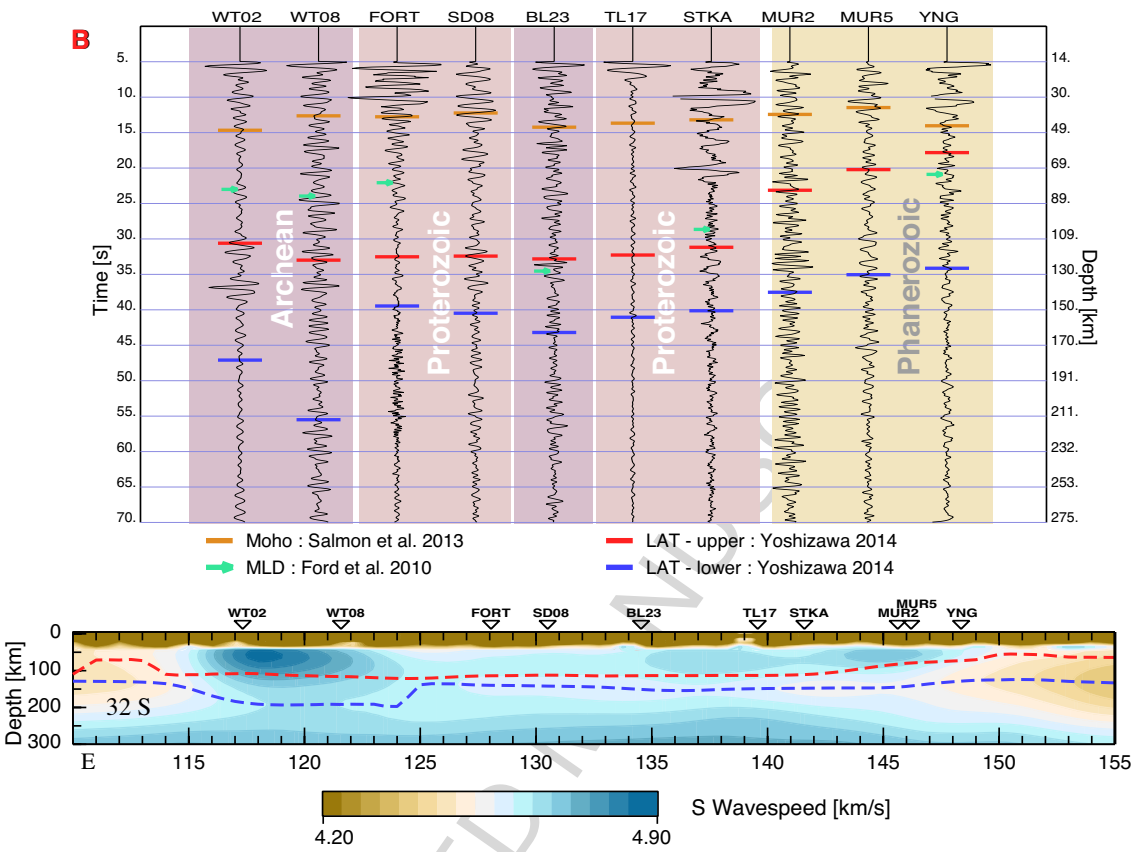

Figure 7: Estimates of *P*-wave reflectivity for stations along the southern profile **B**, for the frequency range 0.6-3.0 Hz extracted from stacked station autocorrelograms.

At each station we also indicate the Moho estimate from the AuSREM model (Kennett and Salmon, 2012), and the LAT bounds from the Yoshizawa (2014) model. The *P* reflectivity shown in Figures 6, 7 is for the frequency band from 0.6-3.0 Hz and indicates the presence of variability on scales from a few hundred meters to tens of kilometers.

The northern profile A (Figure 6) initially crosses the Archean Pilbara craton and then enters the Proterozoic of the Northern Australian craton, and finishes at CTA in the Paleozoic just off the edge of Precambrian outcrop. There are significant differences in the character of reflectivity between stations, but a general consistency in style between tectonic regions. Thus the reflectivity at both temporary stations (LP05, RP01) and a permanent station (MBWA) on the Archean have a similar appearance with a apparent reflectivity that tends to

diminish with increasing time (depth). Whereas the stations on the Proterozoic of the North Australian craton show strong variability to considerable depth, most likely including localized scattering (Kennett, 2015). This change in character indicates that the heterogeneity regimes are somewhat different. The lithosphere beneath CTA is much thinner and there is a sharp drop in reflectivity below 70 km depth that probably indicates a sharp base to the lithosphere. Interestingly, the reflectivity resumes from 120 km depth as the *S* wavespeed increases out of the pronounced low velocity zone in the asthenosphere.

The southern profile B (Figure 7) crosses a more complex mixture of tectonic environments. In the west WT02, WT08 lie on the Archean Yilgarn craton, then the stations FORT, SD08 lie on a cryptic lithospheric block with no exposure that is of Proterozoic age (confirmed with recent basement drilling). The profile then crosses the South Australian craton that has elements of Archean age, but which has had extensive volcanic intrusives, and grades into Proterozoic in the east. The easternmost stations lie in the Paleozoic Lachlan Fold Belt. The Archean stations are similar to those seen on profile A. However, the character of apparent reflectivity at the Proterozoic stations is notably different from those on the North Australia craton with much weaker reflection returns at greater times.

Such reflectivity estimates are available for more than 200 broad-band portable or permanent stations across the continent, and taken overall there is a tendency for a slight change in the style of reflection response to be associated with the zone of the lithosphere-asthenosphere transition. This change would be consistent with the suggestion of Thybo (2008) of a different heterogeneity regime in the low velocity zone beneath the highest lithospheric wavespeeds.

On Figures 6, 7 we mark the estimates of discontinuities from the *S*-wave receiver function study of Ford et al. (2010), where available, which were interpreted either as the mid-lithosphere discontinuity (MLD) or as the lithosphere-asthenosphere boundary (LAB). Often the indicator from the work of Ford et al. (2010) coincides with a change in reflectivity, but no consistent criteria emerges that might be used to recognize a comparable feature at other

stations. Though, on the southern profile B, we see a tendency for the indicator to fall near a change in the apparent frequency of the reflectivity. In Section 5 we look more closely at the lithospheric discontinuities for a profile of stations in central Australia and show that changes in *P*-reflectivity can be tracked across nearby stations to recognise a 'mid-lithospheric discontinuity'.

3. Multi-scale lithospheric heterogeneity

In Figures 4-6 we have shown the large scale structures in the upper mantle determined from surface-wave tomography, and the presence of fine-scale features from analysis of higher frequency body waves (Figurex 1, 7. Where dense observations are available, as in southeastern Australia, body wave tomography demonstrates the presence of considerable complexity beneath the crust (e.g., Rawlinson et al., 2014) with variations down to the available sampling of 50 km.

Kennett and Nolet (1990) examined the effect of such medium scale heterogeneity superimposed on broad-scale features using a mode-coupling scheme, and demonstrated that the additional heterogeneity is largely transparent to the lower frequency waves employed in surface wave tomography, and so the large-scale results are not affected. Thus a full description of the state of the lithosphere needs to include a broad range of structural features from the broad-scale down to the fine-scale.

Body-wave tomography exploiting dense station sampling in Australia is currently confined to the southeast, though further instrument deployments have recently been extended into Queensland. The tomographic results indicate similar scales of variation in cratonic and Phanerozoic areas. Thus it is reasonable to assume that such medium scale features are likely to be present across the entire continent. In the absence of full continental coverage, the best description that can currently be provided is a stochastic one represented through a few parameters. A similar situation arises for the description of finer-scale variations.

Kennett and Furumura (2016) have built up a composite model for the lithosphere incorporating the full range of scales. They use a set of vertical

slices across the Australian continent (Figure 2) for numerical simulation of seismic wave propagation. Attention is restricted to 2-D profiles since the high frequencies (up to 10 Hz) in the observations are computationally challenging. This multi-scale heterogeneity model was developed progressively starting with the broad-scale structure in the mantle from the AuSREM model (Kennett et al., 2013), and then adding in stochastic representations of medium-scale features, based on the character of structures found in southeastern Australia (see, e.g., Rawlinson et al., 2014). The heterogeneity spectra are specified by a von Karmán distribution with a Hurst exponent of 0.5, which provides strong influence from shorter wavelengths. The fine-scale components were included after extensive testing for both correlation length and amplitude of variability for different parts of the model. The nature of the medium- and fine-scale stochastic features are summarized in Table 1.

This multi-scale model includes significant variation in the crust with larger amplitudes between 15 km depth and the Moho. The lithospheric mantle is mildly heterogeneous with a longer horizontal correlation length, which is needed to produce the minutes of coda duration for both *P* and *S* waves for passage through the Precambrian zones. Between the lithosphere-asthenosphere transition (LAT) bounds extracted from the model of Yoshizawa (2014) a change in heterogeneity regime is imposed with larger amplitude and shorter horizontal correlation length (cf. Thybo, 2008). In the asthenosphere beneath the deeper LAT bound the same style of heterogeneity is sustained. The composite heterogeneity model includes features of the full-range of models proposed for fine-scale heterogeneity in Eurasia. The multi-scale model confirms the strong influence of the slower varying background structures, and the importance of variations in the vertical and horizontal gradients of wavespeed (cf. Morozova et al., 1999).

This composite model with many different scales of heterogeneity in various depth ranges gives rise to a rich structure with a slow decline in the wavelength spectrum (Kennett and Furumura, 2016, Figure 4). In 2-D simulations it is able to produce a good representation of the character of high-frequency wave

Table 1: Heterogeneity regimes used in multi-scale model: amplitudes and correlation lengths.

Medium-scale

Depth range	r.m.s. het.	horiz. correl.[km]	vert. correl. [km]
0-300 km	1%	100	24

Fine-scale

Depth range	Label	r.m.s. het.	horiz. correl. [km]	vert. correl. [km]
0-15 km	C1	0.5%	2.6	0.4
15-Moho km	C2	1.5%	2.6	0.4
to top LAT	L1	0.5%	10.0	0.5
LAT	L2	1.0%	5.0	1.0
Asthenosphere	A	1.0%	5.0	1.0

propagation out to 1800 km across the continent, and also the correlation properties of seismic waves across the PSAR array in northwestern Australia from an event in central Australia (Kennett and Furumura, 2016).

3.1. Numerical simulation of the seismic wavefield

The finite-difference-method (FDM) simulations of Kennett and Furumura (2016) have been carried out using a fourth-order, staggered-grid, scheme in space and second-order in time, with an efficient parallelisation scheme (Furumura and Chen, 2004) that sustains high accuracy for long distance seismic wave propagation at high frequencies (up to 10 Hz). The computational domain for the 2-D profiles is 2580 km wide and 288 km deep, discretized with a uniform grid interval of 0.1 km. Earth flattening is applied to the *P* and *S* wavespeeds in order to include the effect of the sphericity of the Earth using a conventional rectangular-grid FDM. The calculations include allowance for attenuation using a broad-band Q model, with nearly constant Q_p and Q_s in a frequency band from 0.5 to 5 Hz. A double-couple line source with 45-degree dip angle is placed at a depth

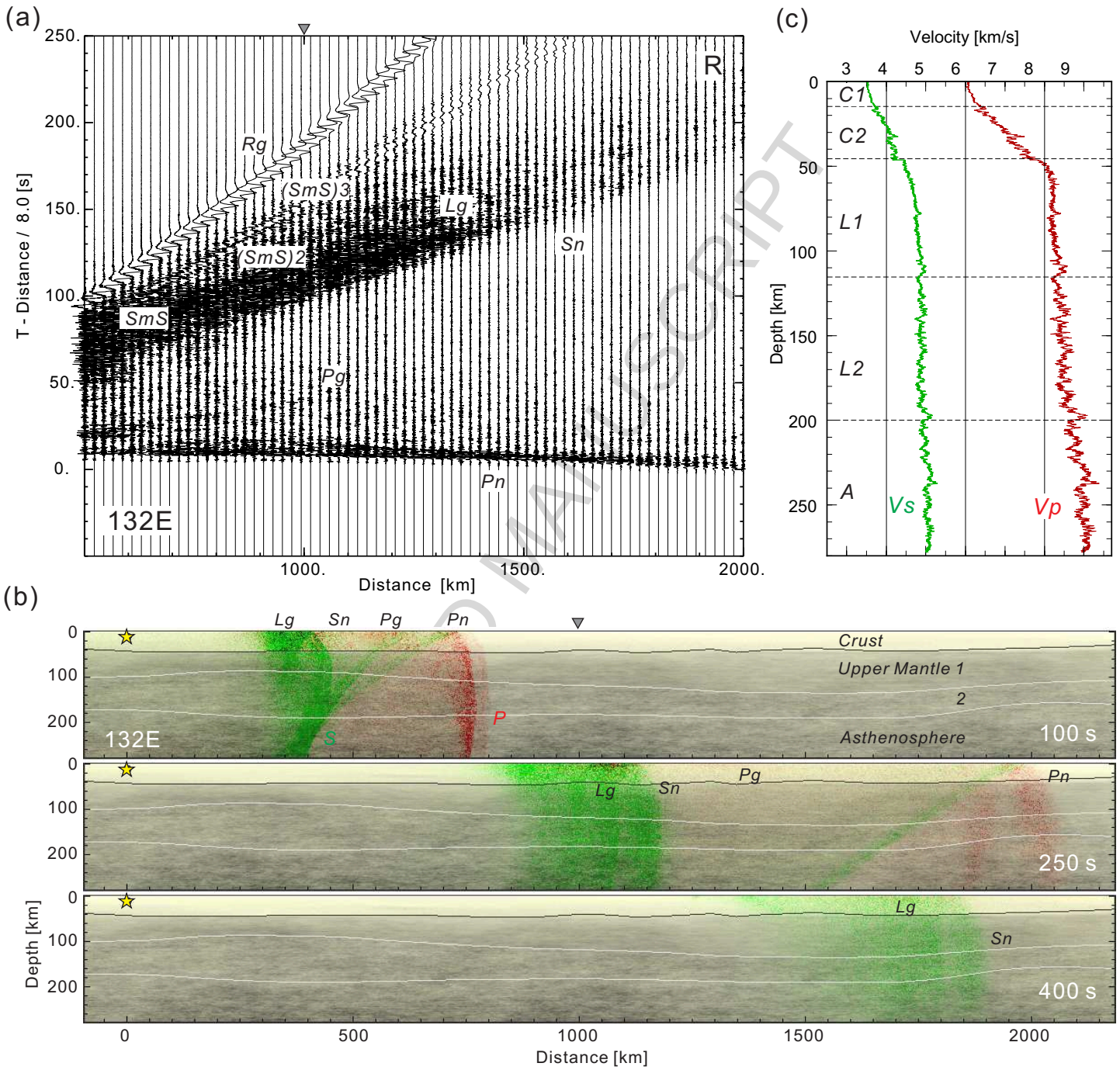

Figure 8: Simulation of the effect of propagation along a 2-D profile at 132°E with the inclusion of the broad-scale structure from AuSREM, stochastic medium scale heterogeneity, and the addition of fine scale heterogeneity throughout including the asthenosphere: (a) radial theoretical seismograms for propagation to 2000 km; (b) snapshots of the wavefield for a source in the west, with *P* waves indicated in red and *S* waves in green; (c) 1-D profile through the heterogeneous model at 1000 km (flattened).

of 10 km, with a source-time function consisting of a pseudo-delta function that radiates seismic waves with a maximum frequency of 6 Hz; this ensures stability of the wavefield throughout the domain. The propagation of the high-frequency, scattered *P* and *S* wavefields for larger distances (>500 km) has little sensitivity to the details of the source mechanism.

From the FDM simulation we display synthetic seismograms of the radial (R) ground velocity at the surface, together with snapshots of the seismic wavefield for selected time steps (Figure 8). The *P* and *SV* contributions in the snapshots are separated by taking the divergence (*P*) and curl (*SV*) of the 2-D wavefield.

The wavefield generated by the crustal source in the multi-scale heterogeneity model is complicated, with both distinct seismic phases and elongated codas comparable to the observations. In Figure 7 we illustrate the nature of seismic wave propagation though a 2-D profile along 132°E. We show a dense record section of seismograms and snapshots of the wavefield for a source in the north. This profile along 132°E lies mostly through Proterozoic domains. It starts in the North Australian craton (to 900 km) traverses the suture zone in Central Australia and then passes into the South Australian craton and its offshore extension (from 1500 km). The LAT is somewhat thicker in the north, and the shallower boundary deepens after the North Australian craton has been traversed.

Along the 132°E profile there are significant gradients in *P* and *S* wavespeed below relatively thick crust. The refracted phase *Pn* is quite strong, with reinforcement from the surface reflection *pPn*. The character of the arrival varies noticeably along the profile, but consistently has a long coda with significant high-frequency energy persisting for 2 min of more beyond 1500 km epicentral distance. The *S* wavefield is particularly complex out to 1500 km, with the coda of *Sn* interfering with crustal *S* multiples to build a long sustained *Lg* phase with a rather high group speed. At larger distances the large scale velocity contrasts and changes in velocity associated with the South Australia craton lead to a noticeable change in the complexity of the *S* phases, but still there is a long high-frequency coda.

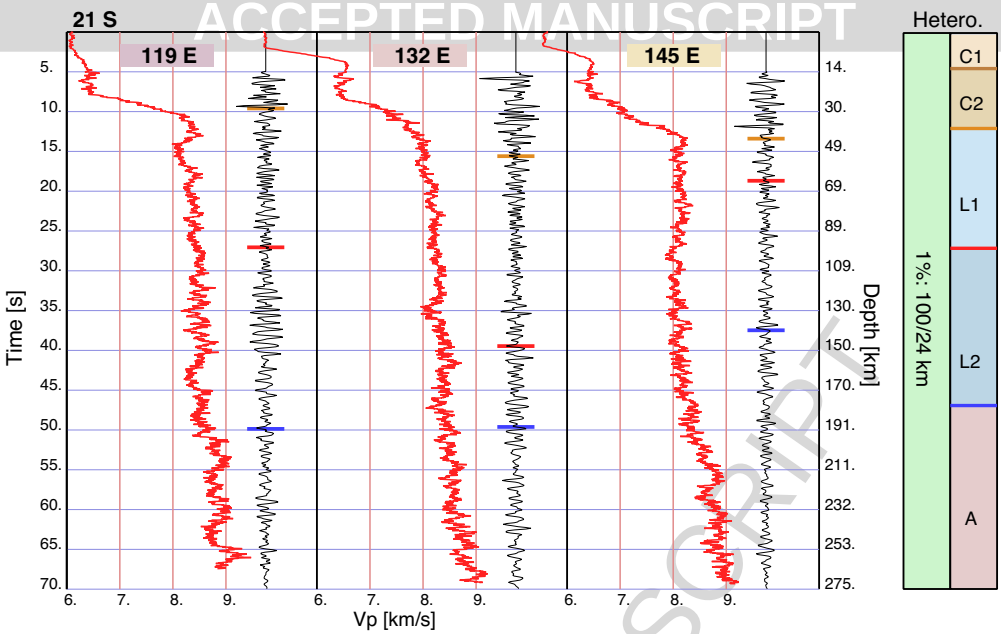

Figure 9: Autocorrelograms of transmitted *P* waves through 1-D models extracted from a 2-D multi-scale heterogeneity model for 21°S (Kennett & Furumura, 2016). For each position the flattened *P*-wave velocity model is shown as a function of time to the left, and the autocorrelogram results to the right. The indicators for the depth to Moho and the upper and lower bounds on the lithosphere/asthenosphere transition are placed as for the observations. In the right-hand panel we show the various heterogeneity regimes applied in the construction of the multi-scale models (see Table 1).

Somewhat similar behaviour is seen for simulated propagation on a profile along 119°E for a northern source (Kennett and Furumura, 2016, Figure S7), though on this profile the *Pn* train is more complex, and the more gentle variations in larger scale structure means that there is only a slow decay in the amplitude of the *S* wave train. Whereas for a profile along 145°E (Kennett and Furumura, 2016, Figure S9), which has both thinner lithosphere and significant gradients in structure, the high-frequency coda of both *P* and *S* decays quite rapidly. *Sn* is weak beyond 1300 km, which is in accord with the pattern of observations for eastern Australia events.

3.2. Receiver based results

The results from the stacked autocorrelograms at the stations across Australia show a distinct contrast between the strong level of apparent *P*-wave reflectivity in the crust and the lower level in the mantle component of the lithosphere (Figures 6, 7). We can gain insight into interactions between different scales of heterogeneity

in the creation of the reflectivity traces by examining a set of detailed 1-D models extracted from the multi-scale heterogeneity model, with character representative of different geologic provinces

These complex 1-D models are very finely layered with vertical sampling of 0.1 km. Incident *P* waves are introduced at the base of the structure at 280 km with small slownesses, and the transmission response including the effect of the free surface is constructed. The autocorrelation of the vertical component of the synthetics seismograms for the transmitted waves is then calculated to extract the *P*-wave reflection response, as presented by Gorbatov et al. (2013). A stack of the reflectivity is made over 5 slownesses out to 0.01 s/km, and then the resultant trace is band pass filtered in the band 0.5–3.0 Hz. This process is designed to follow the steps used for the observations, and so allow direct comparison with the results in Figures 6 and 7.

As can be seen from Figure 9, synthetic *P*-wave reflectivity traces created in this way closely resemble the stacked station results in Figures 6, 7. We show results for three locations along 21°S where the grid of numerical simulations intersect. Alongside each trace we display the *P* wavespeed distribution for the 1-D model at that location. The interaction of the multiple heterogeneity scales produces complex fine-grained structure throughout the lithosphere and asthenosphere. Although major contrasts in *P* wavespeed have a direct expression in the reflection traces, many complex reflectivity features arise from interference effects. This is similar to the situation in standard reflection seismology with changes in cyclic bedding in sedimentary sequences or where thin coal layers are present.

The contrast in reflectivity style between the crust and the lithospheric mantle in Figure 9 is similar to that seen at many of the stations shown in Figure 6. The 1-D model at 119°E is representative of Archean structure, with a broad lithosphere-asthenosphere transition (LAT). The synthetic reflectivity from this LAT zone is somewhat larger than that seen at the stations LP05, RP01 and MBWA on Profile A (Figure 6). The model at 132°E, lies in the Proterozoic

domain; the reflectivity is a little less than seen for comparable stations on Profile A, but cannot include any 3-D scattering effects. At 145°E the 1-D model represents the Phanerozoic belt with a thin zone of higher wavespeeds.

The results from these 1-D models indicate that near vertical propagation through complex, but realistic, heterogeneity can reproduce much of the character of the stacked autocorrelograms, and provide a useful constraint on likely levels of variation in the lithosphere.

3.3. Sampling of heterogeneity

We can gain insight into the way that observational probes sample the lithosphere from the multi-scale heterogeneity model. In Figure 10 we show two segments of the 2-D heterogeneous representation along 26°S at 119°E in the Archean Yilgarn craton with thick lithosphere and at 145°E in the Phanerozoic domain where shear wavespeeds are lower and the lithosphere is beginning to thin. The contribution to the *P*-wave reflectivity estimates from distant earthquakes will sample a broad swath of structure beneath a station as indicated by the yellow lines in Figure 10. The stacking of the station autocorrelograms segments will lead to averaging of structure, which will encompass a wider domain at greater depth. This means that the apparent reflectivity for the crust and immediate uppermost mantle will closely resemble the 1-D profile below the receiver. At greater depth averaging will span similar, but not identical structures, and so the apparent variations in depth will be blurred. A natural consequence is that we expect the *P*-wave reflectivity to diminish in amplitude and become slighter lower frequency at later times. Situations where clear higher frequency energy appears at late time imply locally strong horizontal continuity. An interesting example is provided by station FORT (profile B - Figure 7) where high-frequency arrivals are seen for depths below 160 km in the asthenosphere. This suggests a finely laminated asthenosphere with structure with horizontal correlation lengths of 50 km or more.

When we make 1-D simulations of *P*-wave reflectivity, as in Figure 9, we can therefore expect that we will overemphasize deeper structure relative to any

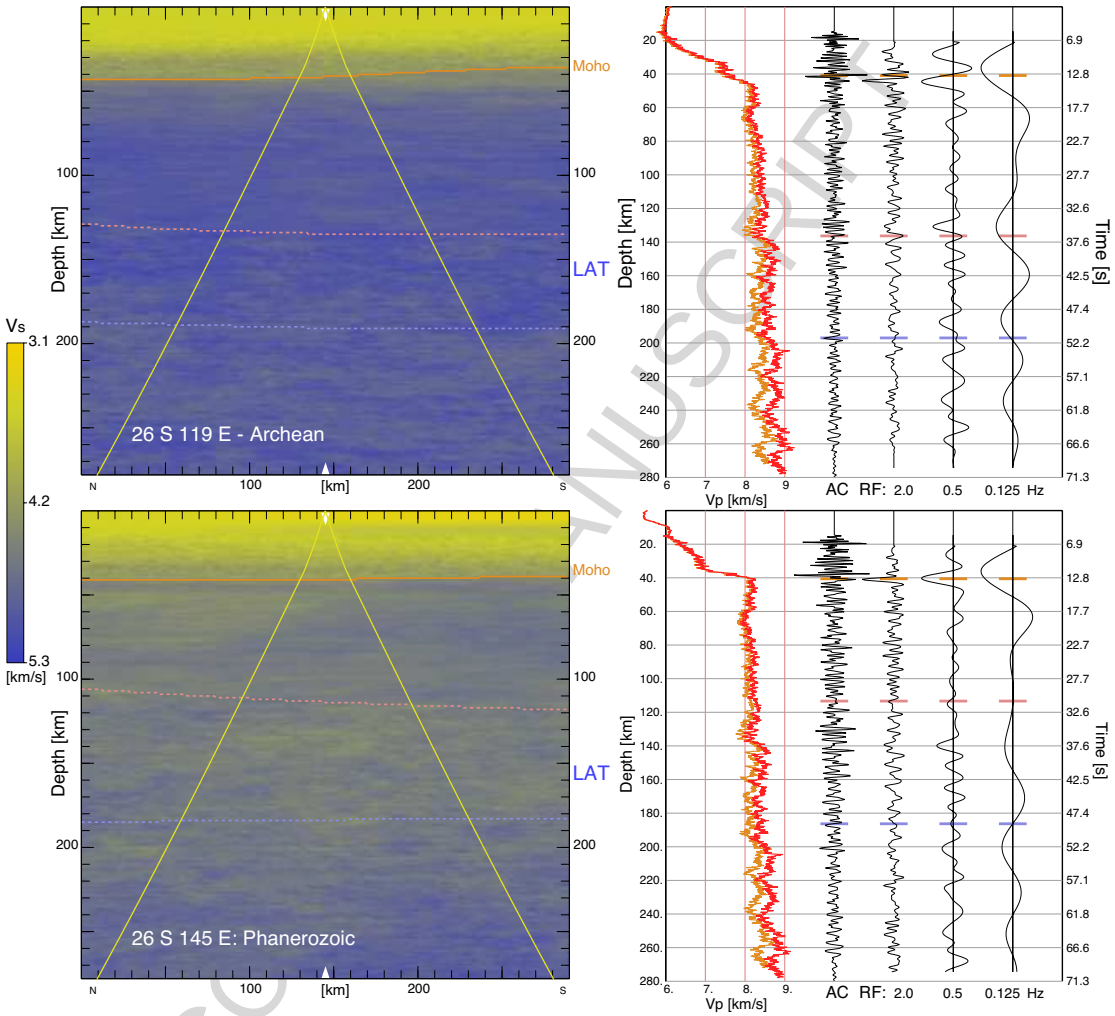

Figure 10: 2-D heterogeneity segments at 119°E and 145°E along 26°S, at true scale. Indicative sampling limits are shown for telecseismic arrivals at central locations. For each location simulations of *P*-wave reflectivity and *Sp* receiver functions for a 1-D model extracted at the central point are shown as a function of depth on the same scale as the heterogeneity model. The flattened model used for the computations is shown in red, and the true velocities in orange to provide a better rendering of the velocity gradients. The *P*-wave reflectivity is extracted from the autocorrelation (AC) of the transmission response in the frequency band 0.6-3.0 Hz. The suite of *Sp* receiver functions (RF) are scaled by depth to match the reflectivity in time, and are shown for a range of band-pass filter settings: 0.05-2.0 Hz; 0.05-0.5 Hz; 0.05-0.125 Hz.

observations for the same 2-D or 3-D heterogeneity structure. Nevertheless, the calculations will provide a good guide to the general behaviour. In Figure 10 we also display the 1-D model for the central location in the heterogeneity spread along with the reflectivity estimated from autocorrelation of transmitted *P* waves.

As well as the autocorrelation we can use the 1-D models to look at the properties of receiver functions for such complex structures. We have therefore constructed *Sp* receiver functions using the same transmission response scheme as used for the *P*-wave reflectivity, with stacking over a bundle of slownesses. Since we are looking at the *P* conversions from an incident *S* wave we can tie the receiver function results to the reflection case through the depth of conversion. Accordingly we present reflectivity and *S* receiver function results for the 1-D models in Figure 10 on a common depth scale, using the *ak135* model for conversion from time. When the *Sp* receiver functions are calculated for high frequencies they have very similar behaviour to the *P*-wave reflectivity, and indeed we can track the same major changes in time behaviour. Reflections and conversion pulses are commonly associated with locations where there is a change in the style of wavespeed variation rather than particular jumps.

When progressively stronger low-pass filtering is imposed on the receiver functions we see considerable change in the apparent behaviour. In the passage from the broadest band traces (0.05-2.0 Hz) to the lowest frequency band (0.05-0.125 Hz) the receiver function records apparently simplify, and just a few apparent discontinuities emerge from an initially very complex pattern. However, the seeming simplicity does not come from distinct changes in seismic wavespeed, but rather the interference of many subtly different arrivals from each of the tiny contrasts in the original wavespeed distribution.

The choice of a 0.05-0.125 Hz frequency band is typical of filtering used in *S*-wave receiver function studies directed at lithospheric studies (e.g., Kind et al., 2012). The time relationships of such traces can indeed be well represented by simple wavespeed distributions with large jumps, but that is not their true origin. Hints of the actual complexity are likely to arise when higher frequencies

are considered and then the single pulses break up into multiple sub-pulses. Such effects have been recognized in recent studies with suggestions of multiple mid-lithospheric discontinuities (Sodoudi et al., 2013; Hopper et al., 2014; Wirth and Long, 2014), though it can be difficult to get enough high-frequency energy in incident *S*.

With the presence of broad-scale and medium-scale structure we can expect modulation of the fine-scale structure so that nearby stations may see broadly similar structures. This will mean that there can be continuity of apparent structure when seen with closely spaced stations, even though there may not be a simple 'discontinuity' being mapped.

3.4. Variations in heterogeneity style

In Figure 10 we have already compared segments of heterogeneity structure, and can see significant differences in the character at 119°E and 145°E. In the Archean domain at 119°E the variations in the longer spatial wavelengths are more muted and so we see more apparent continuity of the fine-scale structure. Whereas, in the Phanerozoic at 145°E we see stronger modulation of the fine-scale structure.

We present a further comparison in Figure 11, where we show three segments taken along the 132°E profile, for which we showed the simulation of the wavefield in Figure 8. The northern segment at 21°S lies in the Proterozoic of the North Australian craton, that at 26°S in the Proterozoic mobile belt of Central Australia and 31°S in the reworked South Australian craton. In each case we have a gentle gradient in background properties and a relatively consistent style of fine-scale structure across the 300 km wide segments, though more variation is apparent in the south at 31°S.

For the rather gradational crust-mantle transition at 21°S, the Moho is apparent as the base of reflectivity. The Moho is distinct for the broader frequency bands in the *Sp* receiver functions, but would be misinterpreted for the lowest frequency band with an exaggeration of crustal depth. At the other locations, the effects are less marked and the Moho depth estimate is quite good across all frequency bands.

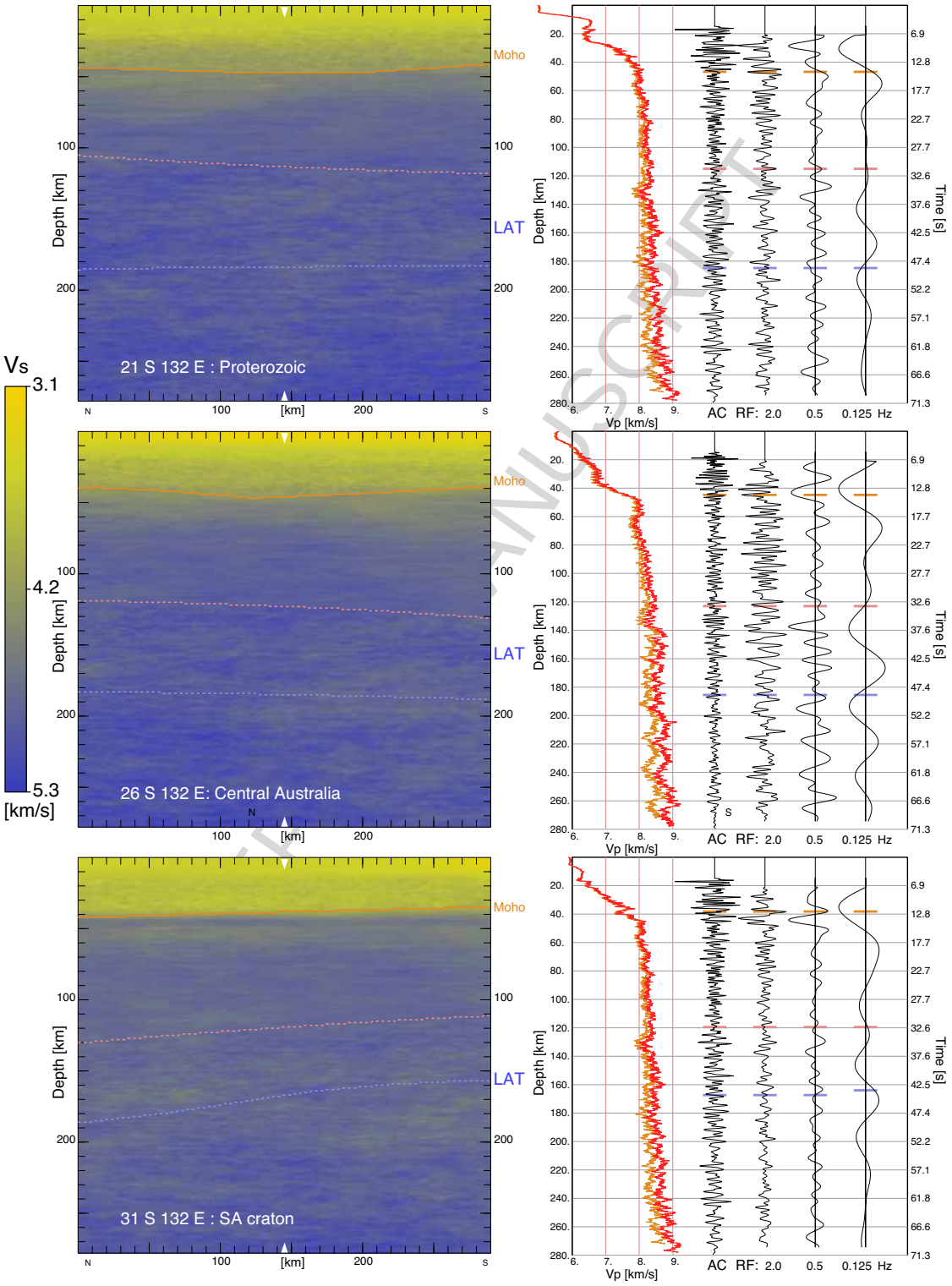

Figure 11: 2-D heterogeneity segments along 132°E at 21°S, 26°S and 31°S, at true scale. For each location simulations of *P*-wave reflectivity and *Sp* receiver functions for a 1-D model extracted at the central point are shown as a function of depth on the same scale as the heterogeneity model. The flattened model used for the computations is shown in red, and the true velocities in orange to provide a better rendering of the velocity gradients. The *P*-wave reflectivity is extracted from the autocorrelation (AC) of the transmission response in the frequency band 0.6-3.0 Hz. The suite of *Sp* receiver functions (RF) are scaled by depth to match the reflectivity in time, and are shown for a range of band-pass filter settings: 0.05-2.0 Hz; 0.05-0.5 Hz; 0.05-0.125 Hz.

For all the heterogeneity segments we see the emergence of a change in reflectivity at or just above the shallow bound on the LAT, where we have made a change in the style of fine-scale heterogeneity. Commonly this translates into an apparent simple feature for the lowest frequency band of the *Sp* receiver function simulations, that tends to breakup into more complex pulses in the higher frequency bands. In each case we are sampling the same structure, the differences arise from selective interference in reverberation and conversion with varying frequency content.

4. Mid-lithospheric discontinuities in Central Australia

For a dense line of seismic stations across the North China craton, Sun and Kennett (2017) have recently demonstrated that it is possible to track a coherent 'mid-lithosphere discontinuity' (MLD) across estimates of *P*-wave reflectivity extracted from auto-correlograms of the immediate coda of teleseismic *P* waves. This work used spatial stacking with the dense data to enhance lateral coherence, and then picked the MLD by changes in local frequency on the reflectivity traces. Along this line the thickness of the lithosphere varies considerably, but the MLD generally marks the depth at which tomography indicates the beginning of a reduction in shear wavespeed.

Although in Australia there is no comparably dense set of stations, we can make use of the 2008-2010 BILBY deployment in Central Australia with 25 stations at approximately 50 km spacing to look at the mantle discontinuities. Sippl (2016) has exploited *P* receiver functions to image the strong variations in crust structure along the profile. Here we use the stacked station autocorrelograms to examine patterns in *P* reflectivity along the BILBY stations and nearby permanent stations (AS13, WRAB). The stations employed are indicated by the light blue symbols in Figure 2. We display in Figure 12 the *P* reflectivity estimates superimposed on the radial anisotropy (ξ) and isotropic shear wavespeed from the model of Yoshizawa (2014). We project the stations on to 134°E for the north-south line and 19.6°S for the smaller west-east line. The reflectivity traces

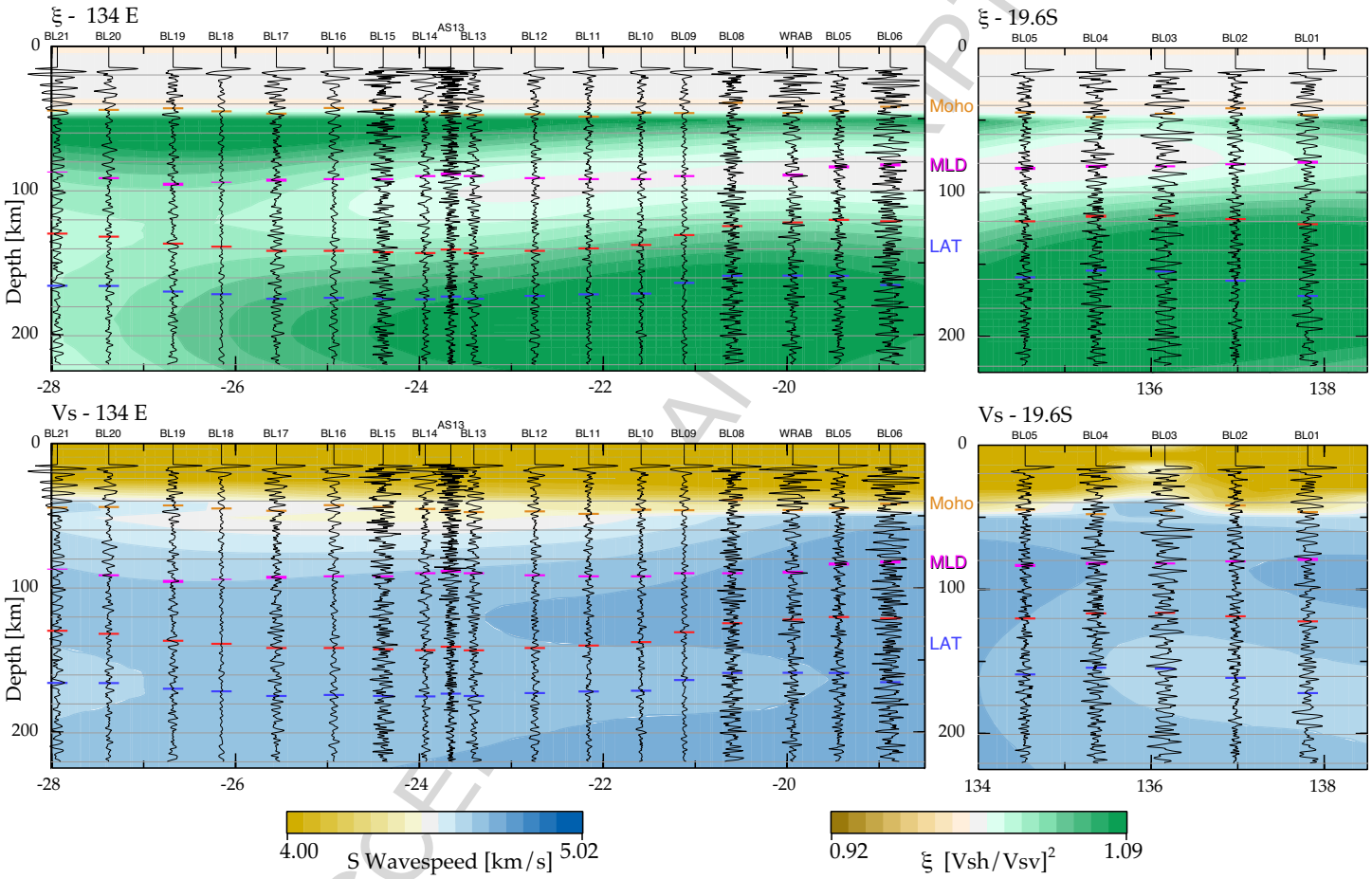

Figure 12: *P*-wave reflectivity estimates from stacked station autocorrelations for a profile of closely spaced seismic stations in central Australia projected onto the meridian 134°E, and parallel 19.6°S. The background is provided by the radial anisotropy (ξ) and isotropic *S* wavespeed models from Yoshizawa (2014). The depth to the Moho and the shallow and deeper bound on the lithosphere-asthenosphere transition (LAT) are indicated. Also marked is an estimate of the location of a mid-lithosphere discontinuity (MLD) based on change in frequency character in the *P*-wave reflectivity.

are converted to depth using the *ak135* model (Kennett et al., 1995) so that they can be directly compared to the anisotropy and velocity sections. The depth to the Moho and the shallow and deeper bounds on the lithosphere-asthenosphere transition are shown at each station.

For each station in Figure 12, we also mark in purple the position of a mid-lithosphere discontinuity marked by a change in the apparent frequency of the reflectivity. Both manual picking and calculations of instantaneous frequency are in very close correspondence (typically $<$1 km). The thickness of the purple line increases with the clarity of the change. AS13 is a single short-period station from the 10 km aperture Alice Springs array (ASAR); a clear change in reflectivity at 90 km depth is seen across all the stations in the array (Kennett, 2015, Figure 3). WRAB is co-located with the 25 km aperture Warramunga Array (WRA); perceptible gradients in crustal structure can be seen on the N-S and E-W arms of this array, but again there is a consistent reflectivity change at 91 km – the depth suggested for the MLD at WRAB from *Sp* receiver function analysis by Ford et al. (2010).

The 'discontinuity' identified by the change in frequency on the reflectivity traces although spatially coherent across the suite of stations does not have a simple relation with the broad-scale wavespeed and anisotropy. For the southern stations the trend of the weak change mirrors the gradient is isotropic *S* wavespeed at the base of a zone of lowered velocities. To the north where the discontinuity is more distinct, its position approximately tracks the minimum in the radial anisotropy parameter ξ; behaviour that tends to mirror the correlation noted by Yoshizawa and Kennett (2015) with the mid-lithosphere discontinuity results obtained by Ford et al. (2010) using *Sp* receiver functions.

The coherent presence of a mid-lithospheric discontinuity in central Australia suggests that in this region there may be the beginnings of a change of heterogeneity style around 90 km depth that becomes more developed in the LAT zone. However, such indications are indirect. The interferences induced by fine structure will always tend to obscure the nature of the variations in physical

properties that produce them.

5. Linking seismic and geochemical heterogeneity

A suite of xenocryst and xenolith sites across southeastern Australia have been subjected to detailed geochemical analysis by Gaul et al. (2003). The results indicate distinctive geochemical stratification both in mineral species and Magnesium number (Figure 13b). The profile of xenoliths traverses from the Galwer component of the South Australian craton, along the southern edge of the Curnamona component and crosses into the Paleozoic Lachlan fold belt at about the location of White Cliffs (Figure 13a).

The analysis of Gaul et al. (2003) presented in Figure 13b is based on the properties of garnets and chromites from each site. The estimate of the equilibrium pressure for individual garnet grains is based on the chromium content of the garnet, and the parent rock type is inferred from CaO-Cr_2O_3 systematics. From a large number of garnet grains a profile of rock type can then be built up as a function of depth - a form of 'chemical tomography'. The Fe/Mg ratio for olivine coexisting with each garnet grain has been extracted using the garnet-olivine Fe-Mg-exchange geothermometer. This allows an estimate of the Mg# (Mg/[Mg+Fe]) as a function of pressure (and thus depth). These geochemical results represent the state of the lithosphere at the time of entrainment of the mantle samples.

These xenolith locations lie within the area in southeast Australia where there have been extensive deployments of temporary seismic stations. We have therefore been able to use the spatial stacking approach of Kennett et al. (2015) to produce *P*-wave reflectivity estimates at each of the xenoliths. The spatial stacks of reflectivity are constructed using a Gaussian with half width 0.5° about the desired site, and typically take in contributions from around 5 stations. In this way we stabilise the reflectivity estimates at the xenolith sites without sacrificing geographic resolution. The area sampled is comparable to that covered in the xenocryst collections. The locations of the xenoliths, and the distribution of

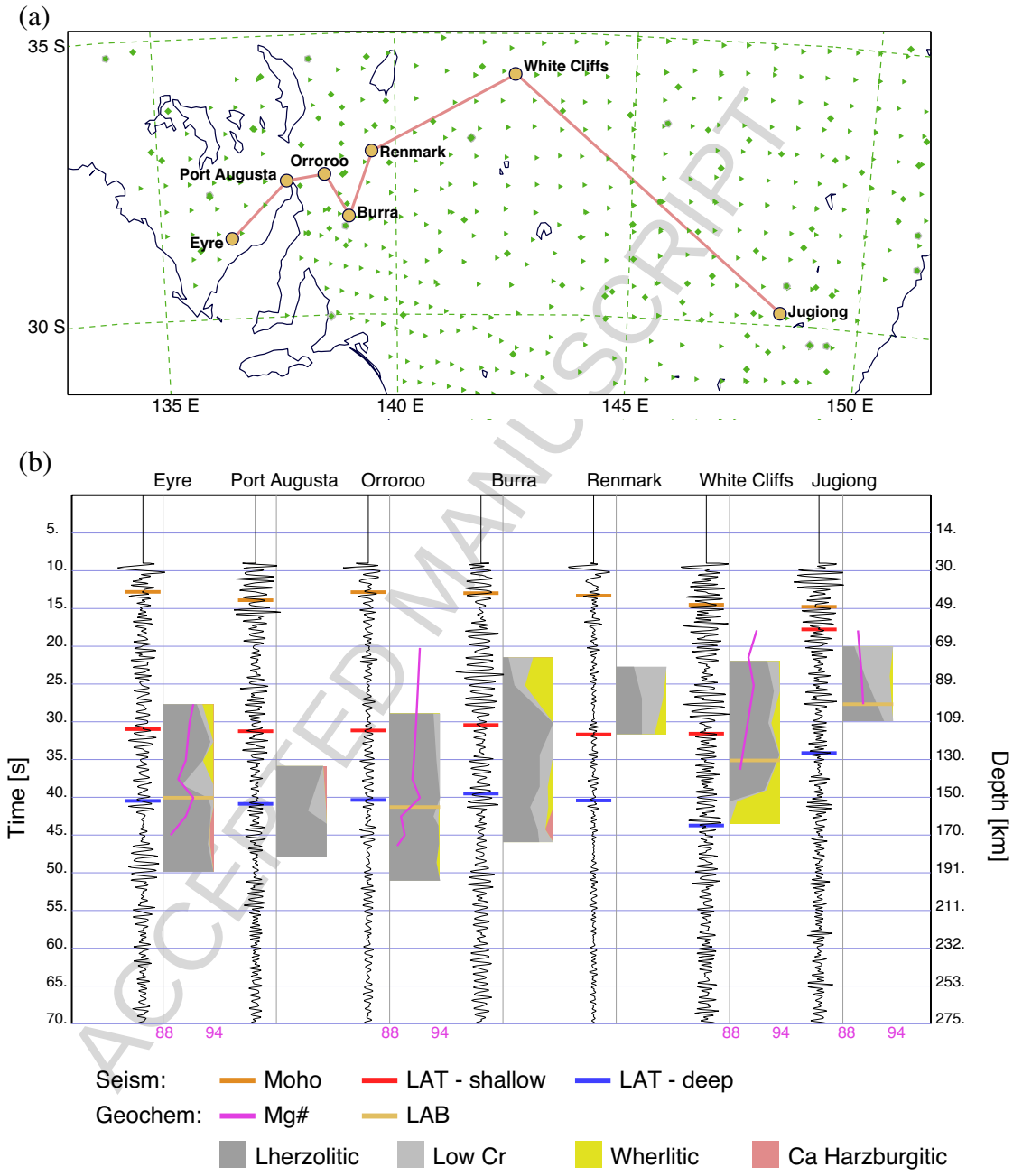

Figure 13: (a) Position of a suite of xenoliths (orange circles) across southeastern Australiarelative to the location of seismic stations (green symbols). Spatial stacks of autocorrelograms are used to provide estimates of *P*-reflectivity at the xenoliths. (b) Comparison of *P*-relectivity estimates at the xenoliths with geochemical variations as a function of depth from Gaul et al. (2003). The range of Magnesium numbers is shown below the xenoliths for which they are available.

available seismic stations are shown in Figure 13a.

In Figure 13b we plot the reflectivity estimates at the xenolith sites alongside the chemical stratification results from Gaul et al. (2003). In each case there has been a conversion to depth. The *ak135* velocity model has been used to convert time to depth for the seismic results. Whereas depth has been inferred from pressure indicators for the geochemical profiles.

In view of the uncertainties in each of the depth conversions, and the time span since the xenolith samples reached the surface, the correspondence of changes in seismic reflectivity with depths where there are notable changes in chemical composition or Magnesium number is striking. The geochemical indicators for the base of the lithosphere (LAB) either coincide with the deep bound on the LAT from seismic tomography (Yoshizawa, 2014) or lie within the span of the bounds. The geochemical LAB tends to lie at or near the base of a burst of apparent reflectivity. Both classes of information are in concord on a progressive thinning of the lithosphere towards the east under the Phanerozoic domain.

These results suggest that there is a direct link between the mineralogical variation detected in the xenoliths, and the depth dependence of seismic properties. Local modifications of the physical properties would contribute to reflectivity and interleaving of mineral assemblages would be an effective way of inducing fine-scale variations in the lithosphere.

6. Discussion

Our observational examples illustrate the complexity of structures encountered within the lithosphere, with clear general trends but considerable local variability. Such features are consistent with the numerical simulations using the multi-scale heterogeneity model. In particular, the presence of medium-scale heterogeneity can produce notable changes between stations at even 50 km spacing.

A diagnostic of the presence of finer-scale structure is a strong frequency dependence of the character of apparent discontinuities. Lower frequencies are frequently preferred because of the relative simplicity of the resulting receiver

functions that appear to be able to be described by a few first-order jumps in wavespeed. If, however, the traces change markedly with inclusion of higher frequencies the apparent simplicity is illusory. Indeed inferences about necessary levels of wavespeed variations may well be overstated with the use of an over-simplified model. For the various examples of 1-D profiles from the multi-scale heterogeneity model, local variations rarely exceed 2%. Yet, the net effect of pulse interference suggests contrasts of 5% or more with a simple jump in wavespeed.

A multi-scale model necessarily implies a wide range of structural features some of which may act as suitable 'discontinuities' when sampled with commonly used frequency bands. The thicker parts of continents can then be *riddled by discontinuities* in the depth range from 90-130 km, as remarked by Cooper et al. (2017). This is the depth range in which changes in heterogeneity style with depth are most likely.

Our multi-scale heterogeneity model has been built from isotropic materials, but it will give rise to an effective anisotropy when sampled by long wavelength waves. A stratified laminate appears to show radial anisotropy for incident lower frequency waves (see, e.g., Fichtner et al., 2013b) with differences between the velocities of vertically and horizontally travelling waves. The situation is more complex for a stochastic quasi-laminar structure. Nevertheless in aggregate the class of structure we have proposed for the upper part of the mantle lithosphere will show radial isotropy. As the aspect ratio between horizontal and vertical correlation lengths reduces there will still be some level of anisotropic effect, but less pronounced. We can expect some contribution from the medium-scale structure, the crust, and the LAT. The combination of all the different aspects of the multi-scale heterogeneity can probably contribute up to half of the radial anisotropy seen in surface wave studies (e.g., Yuan et al., 2011; Yoshizawa, 2014).

As we have seen in the receiver-based examples, the boundary between varying styles of stochastic heterogeneity can act as discontinuities between different classes of anisotropy. We currently have little control on the *grain* of the

lithospheric heterogeneity and if the different regimes were imposed by varying processes there is the possibility of changes in azimuthal anisotropy at the same time as radial anisotropy. A change of heterogeneity style into the top of the lithosphere-asthenosphere transition can thus have the effect of changing local anisotropic properties and modifying the interference between waves sampling the fine structure. Such features can contribute to the creation of an apparent mid-lithosphere discontinuity without there ever having been a major change in seismic wavespeeds. The heterogeneity shift in the LAT could be a contributor to changes in the direction of the fast axis of azimuthal anisotropy with depth (e.g., Debayle et al., 2005; Yuan et al., 2011).

It is interesting to note that receiver function estimates of the depth to the mid-lithosphere discontinuity tend to lie just beneath the zone of highest *S* wavespeeds, but above the maximum gradient picked for the shallower LAT bound. This is where we expect a reduction in *S* wavespeed, and it is possible that the reorganisation of heterogeneity should be placed shallower than the upper LAT bound.

Selway et al. (2015) provide a careful review of the mid-lithosphere discontinuity and possible causes. For seismic information their attention was focussed on how to produce an appropriate level of wavespeed reduction for *S* wavespeeds, and they were unable to provide a satisfactory solution using thermal effects such as grain boundary sliding, or with anisotropy as a general solution. Their preferred mechanism was the introduction of hydrated material, specifically amphibole, e.g., through ponding above metasomatism. We suggest that it is worth adding an additional contributor through a change in heterogeneity regime linked to the decreasing seismic wavespeeds toward the base of the lithosphere with potential anisotropic influences as required by Wirth and Long (2014).

Surface wave tomography images large scale changes in seismic wavespeed that, at depth, largely reflect the major surface tectonic units. Within the cratonic zones very high *S* wavespeeds are reached, which are difficult to explain without major element segregation (e.g., Griffin et al., 2009) associated with depletion

via melting. Compositional effects may also contribute to the medium-scale variations. Minor geochemical components and the trace-element distributions are likely to be more directly linked to the finer-scale variations (e.g., Afonso and Schutt, 2012).

Geochemical sounding of the lithosphere is largely indirect, with limited sampling from xenoliths that suggest significant compositional variability both laterally and vertically in the lithospheric mantle, as illustrated in Section 5. Minor variations associated with variations in depletion, e.g. linked to crustal formation, would contribute to the modest kilometre scale heterogeneity in the uppermost mantle. The depth of the transition in heterogeneity style we have inferred from the analysis of high-frequency seismic waves matches quite well with the upper extent of metasomatism inferred from xenoliths (Griffin et al., 2009). The rapid increase in the inferred level of metasomatism with depth in the geochemical results would suggest a gradient in heterogeneity properties with a stronger modification at the base. Variations in the level of metasomatism could contribute to medium-scale variability through the LAT zone.

We note that estimates of the thickness of the mechanical lithosphere are usually significantly thinner than seismic values, and often lie close to the level where we would place the shallow bound on the lithosphere-asthenosphere transition (LAT). The change in the style of heterogeneity in the LAT that provides a good correspondence between numerical simulations and seismic observations may well be linked to rheological change.

We have used stochastic models with longer horizontal than vertical correlation lengths to describe both fine- and medium-scale heterogeneity. This is a simple parameterization of complex media and does not imply that all features are horizontally oriented, merely that in aggregate the general trend is horizontal. It is possible that in time we will be able to provide deterministic representations of medium-scales, but stochastic forms will remain for finer scales.

7. Conclusions

Multi-scale heterogeneity in the continental lithosphere is required to represent the character of the seismic wavefield in Australia, both with regard to long-distance propagation and to near vertically travelling waves. Superimposed on the broad-scale variations extracted from seismic tomography, including radial anisotropy, there are modest levels of medium- and fine-scale features that can currently only be represented stochastically. Horizontal correlation lengths are longer than those in the vertical direction, and such effects lead to contribution to radial anisotropy when sampled by longer wavelength waves. In the presence of 3-D variations, there is the potential for an azimuthal anisotropic component as well.

The main framework of the lithosphere-asthenosphere transition can be extracted from the surface wave results, with shallower and deeper bounds derived from the vertical gradients of seismic wavespeed. Radial anisotropy tends to be weak in the mid to lower lithosphere, but more pronounced in the upper part of the lithosphere and in the LAT and asthenosphere beneath. The lower zone is likely to be influenced by mantle flow.

Only high frequency probes can reveal the presence of the finer scale structures directly, but they can have a profound role in shaping seismic observations at lower frequencies. Quite subtle changes in the style of velocity variation can induce reflections and conversions. With lower frequency probes interference occurs between waves generated from nearby features, and an apparent discontinuity can appear as the aggregate of fine scale changes. A change of heterogeneity style into the top of the lithosphere-asthenosphere transition, with both increased amplitude of fine-scale variation and a more squat planform of correlation, changes local anisotropic properties and modifies the interference between waves sampling the fine structure. Wave interference can thus contribute to the creation of an apparent mid-lithosphere discontinuity without there ever having been a major change in seismic wavespeeds.

Acknowledgments

We would like to thank Erdinc Saygin who undertook the task of converting seismogram time series to stacked autocorrelograms for over 1200 stations across the Australian continent. This has proved a valuable resource for studying fine seismic structure across the continent.

Part of this study was supported by JSPS KAKENHI Grant Number 26400443 to K.Y., with additional support from the AuScope AuSREM project. The Earth Simulator Center of JAMSTEC is thanked for providing CPU time on the Earth Simulator.

Afonso, J.C., Schutt, D., 2012. The effects of polybaric partial melting on the density and seismic velocities of mantle restites, Lithos 134-135, 289–305.

Becker, T.W., 2012. On recent seismic tomography for the western United States, Geochem. Geophys. Geosyst. 13, Q01W10, doi:10.1029/2011GC003977.

Cawood, P., Korsch, R.J., 2008. Assembling Australia: Proterozoic building of a continent, Precambrian Res. 166, 1-38.

Cooper, C.M., Miller, M.S., Moresi, L., 2017. The structural evolution of the deep continental lithosphere, Tectonophysics 695, 100-121.

Davies, D.R., Rawlinson, N., Iaffaldano, G., Campbell, I. H., 2015. Lithospheric controls on magma composition along Earths longest continental hotspot track, Nature, 525, 511–514,

Debayle, E., Kennett, B.L.N., 2003. Surface wave studies of the Australian region, in *The Evolution and Dynamics of the Australian Plate*, pp. 25–40, eds. D. Müller, D. and R. Hillis, Geol. Soc. Austral. Spec. Publ. 22 and Geol. Soc. Am. Spec. Paper 372.

Debayle E., Kennett, B., Priestley K., 2005. Global azimuthal seismic anisotropy: the unique plate-motion deformation of Australia, Nature 433, 509–512.

Direen, N.G., Crawford, A.J., 2003. The Tasman Line: where is it, what is it, and is it Australia's Rodinian breakup boundary? Austral. J. Earth Sci. 50, 491-502.

Fichtner, A., Kennett, B.L.N., Igel, H., Bunge, H.-P., 2009. Full seismic waveform tomography for upper-mantle structure in the Australasian region using adjoint methods, Geophys. J. Int. 179, 1703–1725.

Fichtner, A., Kennett, B.L.N., Igel, H., Bunge,H.-P., 2010. Full seismic waveform tomography for radially anisotropic structure: new insights into the past and present states of the Australasian upper mantle, Earth Planet. Sci. Lett. 290, 270–280.

Fichtner A., Fishwick S., Yoshizawa K., Kennett B.L.N., 2012. Optimal spherical spline filters for the analysis and comparison of regional-scale tomographic models, Phys. Earth Planet. Inter. 190, 44–50.

Fichtner, A., Trampert, J., Cupillard, P., Saygin, E., Taymaz, T., Capdeville, Y., Villasenor, A., 2013a. Multiscale full waveform inversion, Geophys. J. Int. 194, 534–556.

Fichtner A., Kennett, B.L.N., Trampert, J., 2013b. Separating intrinsic and apparent anisotropy, Phys. Earth Planet. Inter. 219, 11–20.

Fishwick, S., Kennett, B.L.N., Reading, A.M., 2005. Contrasts in lithospheric structure within the Australian Craton, Earth Planet. Sci. Lett. 231, 163–176.

Fishwick, S., 2010. Surface wave tomography: Imaging of the lithosphere-asthenosphere boundary beneath central and southern Africa? Lithos, 120, 63–73.

Ford, H.A., Fischer,K.M., Abt, D.L., Rychert C.A., Elkins-Tanton,L.T., 2010. The lithosphere-asthenosphere boundary and cratonic lithospheric layering beneath Australia from Sp wave imaging, Earth Planet. Sci. Lett. 300, 299-310.

Furumura, T., Chen, L., 2004. Large scale parallel simulation and visualization of 3-D seismic wavefield using the Earth Simulator, Comput. Mode. Eng. Sci., 6, 153-168.

Gaina, C., Müller, D.R., Royer, J.-Y., Stock, J., Hardebeck, J., Symonds, P., 1998. The tectonic history of the Tasman Sea: A puzzle with 13 pieces, J. Geophys. Res., 103, 413–433.

Gaul, O., O'Reilly, S.Y., Griffin, W.L., 2003. Lithosphere structure and evolution in southeastern Australia, in *The Evolution and Dynamics of the Australian Plate*, pp. 185–202, eds. D. Müller, D. and R. Hillis, Geol. Soc. Austral. Spec. Publ. 22 and Geol. Soc. Am. Spec. Paper 372.

Gorbatov, A., Saygin E., Kennett, B.L.N., 2013. Crustal properties from seismic station autocorrelograms, Geophys. J. Int. 192, 861-870.

Griffin, W.L., O'Reilly, S.Y., Afonso J.C., Begg G., 2009. The composition and evolution of lithospheric mantle: a re-evaluation and its tectonic implications, J. Petrology 50, 1185–1204.

Gudmundsson, O., Kennett, B.L.N., Goody, A., 1994. Broadband observations of upper mantle seismic phases in northern Australia and the attenuation structure in the upper mantle, Phys. Earth Planet. Inter. 84, 207–236.

Gung, Y., Panning, M., Romanowicz, B., 2003. Global anisotropy and the thickness of continents, Nature 422, 707-711.

Hammer, P.T.C., Clowes, R.M., Cook, F.A., van der Velden, A.J., Vasudevan K. 2010. The Lithoprobe trans-continental lithospheric cross sections: imaging the internal structure of the North American continent, Canadian J. Earth Sci. 47, 821–857.

Hopper, E., Ford, H.A., Fischer, K.M., Lekić, V., Fouch,M.J., 2014. The lithosphere-asthenosphere boundary and the tectonic and magmatic history of the northwestern United States, Earth Planet. Sci. Lett. 402, 69–81.

Kennett, B.L.N., 1985. On regional S, Bull. Seism. Soc. Am. 75, 1077–1088.

Kennett, B.L.N., Bowman, J.R., 1990. The structure and heterogeneity of the upper mantle, Phys. Earth Planet. Inter. 59, 134–144.

Kennett, B.L.N., Nolet, G., 1990. The interaction of the S wavefield with upper mantle heterogeneity, Geophys. J. Int. 101, 751–762.

Kennett, B.L.N., Engdahl, E.R., Buland, R., 1995. Constraints on seismic velocities in the Earth from travel times, Geophys. J. Int. 122, 108–124.

Kennett, B.L.N., Fishwick, S., Reading, A.M., Rawlinson N., 2004. Contrasts in mantle structure beneath Australia relation to Tasman Lines?, Austral. J. Earth Sci., 51, 563–569.

Kennett, B.L.N., Furumura, T., 2008. Stochastic waveguide in the lithosphere: Indonesian subduction zone to Australian craton, Geophys. J. Int. 172, 363-382.

Kennett, B.L.N., Salmon, M., 2012. AuSREM: Australian seismological reference model, Austral. J. Earth Sci. 59, 1091–1103.

Kennett, B.L.N., Fichtner, A., Fishwick, S., Yoshizawa, K., 2013. Australian Seismological Reference Model (AuSREM): mantle component, Geophys. J. Int. 192, 871–887.

Kennett, B.L.N. 2015. Lithosphere-asthenosphere P-wave reflectivity across Australia, Earth Planet. Science Lett. 431, 225-235.

Kennett, B.L.N., Saygin, E., 2015. The nature of the Moho in Australia from reflection profiling: a review, GeoResJ 5, 74–91.

Kennett, B.L.N., Saygin, E., Salmon, M., 2015. Stacking autocorrelograms to map Moho depth with high spatial resolution in southeastern Australia, *Geophys. Res. Lett.*, 42, 7490–7497.

Kennett, B.L.N., Furumura, T., 2016. Multiscale seismic heterogeneity in the continental lithosphere, Geochem. Geophys. Geosyst. 17, 791–809.

Kennett, B.L.N., Saygin, E., Fomin, T., Blewett, R.S., 2016. *Deep Crustal Seismic Reflection Profiling Australia 1978–2015*, pp v+240, ANU Press.

Kind, R., Yuan, X., Kumar, P., 2012. Seismic receiver functions and the lithosphere-asthenosphere boundary, Tectonophysics 536, 25-43.

Mechie, J., Egorkin, A.V., Fuchs, K., Rydberg, T., Solodilov, L., Wenzel, F., 1993. *P*-wave mantle velocity structure beneath northern Eurasia from long-range recordings along the profile Quartz, Phys. Earth Planet. Inter. 79, 269–286.

Morozov, I.B., Morozova, E.A., Smithson, S.B., Solodilov, L.N., 1998. On the nature of the teleseismic Pn phase observed on the ultra-long-range profile "Quartz" Russia, Bull. Seism. Soc. Am. 88, 62-73.

Morozova, E.A., Morozov, I.B., Smithson, S.B., 1999. Heterogeneity of the uppermost mantle beneath Russian Eurasia from the ultra-long-range profile QUARTZ, J. Geophys. Res. 104, B9, 20 329–20 348.

Myers, J.S., Shaw, R.D., Tyler, I.M., 1996. Tectonic evolution of Proterozoic Australia, Tectonics 15, 1431–1446.

Nielsen, L., Thybo, H., Levander, A., Solodilov, L.N., 2003. Origin of upper-mantle seismic scattering - evidence from Russian peaceful nuclear explosion data, Geophys. J. Int. 154, 196–204.

Nielsen, L., Thybo, H., 2003. The origin of teleseismic *Pn* waves: Multiple crustal scattering of upper mantle whispering gallery phases, J. Geophys. Res. 108, B10, 2460, doi:10.1029/2003JB002487.

Pasyanos, M.E., Masters, T.G., Laske, G., Ma. Z., 2014. LITHO1.0: an update crustal and lithospheric model of the Earth, J. Geophys.Res. Solid Earth 119, 2153-2173.

Rawlinson, N., Salmon, M., Kennett, B.L.N., 2014. Transportable seismic array tomography in southeast Australia: Illuminating the transition from Proterozoic to Phanerozoic lithosphere, Lithos 189, 65–76.

Rychert, C., Shearer, P.M., 2009. A global view of the lithosphere-asthenosphere boundary, Science 324, 495–498.

Salmon, M., Kennett, B.L.N., Stern, T., Aitken, A.R.A., 2013. The Moho in Australia and New Zealand, Tectonophysics 609, 288–298.

Schaeffer, A.J., Lebedev, S., 2013. Global shear-speed structure of the upper mantle and transition zone, *Geophys. J. Int. 194*, 417-449.

Selway, K., Ford, H., Kelemen, P., 2015. The seismic mid-lithosphere discontinuity, Earth Planet. Sci. Lett. 414, 45–57.

Shen, W., Ritzwoller M.H., 2016. Crustal and uppermost mantle structure beneath the United States, J. Geophys. Res. Solid Earth, 121 (6), 4306–4342.

Simons, F.J., van der Hilst, R.D., Montagner, J.-P., Zielhuis, A., 2002. Multimode Rayleigh wave inversion for heterogeneity and azimuthal anisotropy of the Australian upper mantle, Geophys. J. Int. 151, 738-754.

Sippl, C., 2016. Moho geometry along a northsouth passive seismic transect through Central Australia, Tectonophysics 676, 56–69

Sodoudi, F., Yuan, X., Kind, R., Lebedev, S., Adam, J.M.C., Kästle, E., Tilmann, F., 2013. Seismic evidence for stratification in composition and anisotropic fabric within the thick lithosphere of Kalahari Craton, Geochem. Geophys. Geosyst. 14, 5393-5412.

Sun, W., Kennett B.L.N., 2017. Mid-lithosphere discontinuities beneath the western and central North China Craton, Geophys. Res. Lett. 44, 1302-1310.

Thybo, H., Perchuc, E., 1997. The seismic 8 degree discontinuity and partial melting in continental mantle. Science 275, 1626-1629.

Thybo, H., 2008. The heterogeneous upper mantle low velocity zone, Tectonophysics 416, 53–79.

Tittgemeyer, M., Wenzel, F., Fuchs, K., Ryberg, T., 1996. Wave propagation in a multiple-scattering upper mantle; observations and modelling, Geophys. J. Int. 127, 492-502.

van der Lee, S., 2002. High-resolution estimates of lithospheric thickness from Missouri to Massachusetts, USA, Earth Planet. Sci. Lett., 203, 15–23.

Warner, M., Morgan, J.,Barton, P., Morgan, P., Price, C., Jones, K., 1996. Seismic reflections from the mantle represent relict subduction zones within the continental lithosphere, Geology 24, 39–42.

Wirth, E.A., Long, M.D., 2014. A contrast in anisotropy across mid-lithospheric discontinuities beneath the central United States – a relic of craton formation, Geology 42, 851–854.

Yoshizawa, K., 2014. Radially anisotropic 3-D shear wave structure of the Australian lithosphere and asthenosphere from multi-mode surface waves, Phys. Earth Planet. Inter. 235, 33–48.

Yoshizawa, K., Ekström, G., 2010. Automated multimode phase speed measurements for high-resolution regional-scale tomography: application to North America, Geophys. J. Int. 183, 1538–1558.

Yoshizawa, K., Kennett, B.L.N., 2002a. Non-linear waveform inversion for surface waves with a neighbourhood algorithm—application to multimode dispersion measurements, Geophys. J. Int. 149, 118–133.

Yoshizawa, K., Kennett, B.L.N., 2002b. Determination of the influence zone for surface wave paths, Geophys. J. Int. 149, 440–453.

Yoshizawa, K., Kennett, B.L.N. 2004. Multimode surface wave tomography for the Australian region using a three-stage approach incorporating finite frequency effects, J. Geophys. Res. 109 B02, 310, doi:10.1029/2002JB002254.

Yoshizawa, K., Kennett, B.L.N., 2015. The lithosphere-asthenosphere transition and radial anisotropy beneath the Australian continent, Geophys. Res. Lett. 42, 3839-3846, doi:10.1002/2015GL063845.

Yuan, H., Romanowicz, B., Fischer, K.M., Abt, D., 2011. 3-D shear wave radially and azimuthally anisotropic velocity model of the North American upper mantle, Geophys. J. Int. 184, 1237–1260.

Highlights

- Interactions between multiple scales of heterogeneity have a strong influence on the seismic wavefield
- Broad-scale and medium-scale structure from tomography
- Finer-scales supported by observations of varying P-wave reflectivity across the continent
- Vertical changes in character of fine-scale structure produce apparent discontinuities